

Dyonic black bounce solutions in General Relativity

Ednaldo L. B. Junior,^{1,2,*} José Tarciso S. S. Junior,^{3,†} Francisco S. N. Lobo,^{4,5,‡}
Manuel E. Rodrigues,^{3,6,§} Luís F. Dias da Silva,^{4,¶} and Henrique A. Vieira^{3,**}

¹*Faculdade de Física, Universidade Federal do Pará,
Campus Universitário de Tucuruí, CEP: 68464-000, Tucuruí, Pará, Brazil*

²*Programa de Pós-Graduação em Física, Universidade Federal do Sul e Sudeste do Pará, 68500-000, Marabá, Pará, Brazil*

³*Faculdade de Física, Programa de Pós-Graduação em Física,
Universidade Federal do Pará, 66075-110, Belém, Pará, Brazil*

⁴*Instituto de Astrofísica e Ciências do Espaço, Faculdade de Ciências da Universidade de Lisboa,
Edifício C8, Campo Grande, P-1749-016 Lisbon, Portugal*

⁵*Departamento de Física, Faculdade de Ciências da Universidade de Lisboa,
Edifício C8, Campo Grande, P-1749-016 Lisbon, Portugal*

⁶*Faculdade de Ciências Exatas e Tecnologia, Universidade Federal do Pará,
Campus Universitário de Abaetetuba, 68440-000, Abaetetuba, Pará, Brazil*

(Dated: February 20, 2025)

This work explores dyonic black bounce (BB) solutions within the framework of General Relativity (GR), coupled with nonlinear electrodynamics (NLED) and scalar fields (SFs). Previous research has employed NLED and SFs to obtain BB solutions in GR; however, these solutions typically assume the presence of either magnetic monopoles or electric charges exclusively as components of the Maxwell-Faraday tensor. In this study, we examine static and spherically symmetric BB solutions that incorporate both magnetic and electric components, forming what are known as dyon solutions. A dyon is a particle characterized by the coexistence of both magnetic and electric charges. We determine the NLED Lagrangian density and the scalar field potential that produce these solutions and analyze the associated gravitational configurations, focusing on horizons, the behavior of the metric function, and spacetime regularity as described by the Kretschmann scalar. Notably, we present the first BB solution derived from the coupling of a linear electromagnetic Lagrangian and a scalar field with an associated potential as the matter source. This work broadens the class of non-singular geometries in the literature and opens new avenues for investigating dyonic BB solutions within the context of other modified gravity theories.

I. INTRODUCTION

The theory of General Relativity (GR), introduced by Albert Einstein in 1915 [1], stands as one of the most profound achievements in modern physics and is widely regarded as the most successful theory of gravity due to its remarkable agreement with experimental observations and predictions. GR fundamentally redefined our understanding of gravity, describing it not as a force but as the curvature of spacetime induced by mass and energy. This revolutionary framework has provided the foundation for numerous groundbreaking discoveries. Among its early triumphs was the explanation of the anomalous precession of Mercury's perihelion, an observation that had puzzled astronomers for decades and was resolved elegantly within the GR framework [2]. Another significant success was the prediction and subsequent observation of the bending of light by massive objects, a phenomenon confirmed during the solar eclipse of 1919 [3]. These early validations of GR solidified its status as

a robust theory of gravitation. In the modern era, GR has continued to prove its predictive power. The direct detection of gravitational waves by the LIGO and Virgo collaborations in 2015 [4, 5] provided an unprecedented confirmation of Einstein's theory, showing its ability to describe dynamic and extreme astrophysical events such as black hole mergers. Similarly, the Event Horizon Telescope (EHT) collaboration captured horizon-scale images of the supermassive black holes at the centers of the M87 galaxy and the Milky Way [6, 7], offering visual evidence of spacetime curvature near these exotic objects.

Despite its remarkable successes, GR is not without significant challenges. Central to these is its prediction of singularities, regions where the curvature of spacetime becomes infinite, and the equations of GR break down, losing their physical applicability. Singularities arise in critical scenarios, such as the Big Bang, which marks the initial state of the universe, and the cores of black holes. The latter, first described by Karl Schwarzschild in 1916 [8], are modeled as objects characterized solely by their mass, enclosed by an event horizon, a boundary beyond which not even light can escape due to the immense gravitational curvature. However, the Schwarzschild solution, like other classical black hole solutions in GR, is plagued by a central singularity where the laws of physics break down. Resolving these singularities remains one of the most pressing challenges in modern gravitational physics. A complete theory of gravity must not only describe the

* ednaldobarrosjr@gmail.com

† tarcisojunior17@gmail.com

‡ fslobo@ciencias.ulisboa.pt

§ esialg@gmail.com

¶ fc53497@alunos.fc.ul.pt

** henriquefisica2017@gmail.com

dynamics of spacetime but also address these pathologies, ensuring that physical laws remain valid under all conditions. This challenge has driven substantial efforts to extend or modify GR, aiming to create a more comprehensive framework that eliminates singularities and deepens our understanding of gravity’s fundamental nature. One avenue for advancing this understanding involves coupling Einstein’s equations with electromagnetism. This approach enables the exploration of how spacetime interacts with electromagnetic fields, revealing phenomena such as charged black holes and the unique properties they exhibit. By integrating electromagnetism into the equations of GR, we gain access to a rich variety of solutions, providing new insights into the interplay between gravitational and electromagnetic interactions in extreme astrophysical and cosmological settings.

In fact, an innovative approach to addressing the singularities inherent in Maxwell’s classical theory of electrodynamics was proposed by Born and Infeld in 1934 [9, 10]. They extended Maxwell’s framework to eliminate the singularities associated with a point charge and the infinite self-energy of such charges. This groundbreaking work led to the formulation of Nonlinear Electrodynamics (NLED), a theory that modifies the behavior of electromagnetic fields at high intensities. The Born-Infeld model set a foundation for further advancements, including significant contributions inspired by quantum field theory, such as the seminal Euler-Heisenberg theory [11]. Plebanski further expanded the theoretical framework of NLED, offering a broader generalization of its principles [12]. Subsequent developments, such as those by Kruglov and others, have continued to refine and extend NLED, exploring its implications across various contexts [13–16]. In 1968, a landmark advancement in black hole physics was introduced by Bardeen, who proposed the first regular black hole solution, one that avoids the central singularity traditionally associated with such objects [17]. This pioneering concept laid the groundwork for a new class of solutions in gravitational theory. Decades later, the work of Ayon-Beato and García demonstrated that Bardeen’s solution could be derived as an exact solution of GR when the black hole’s matter source was described using NLED [18]. In their interpretation, the regularization parameter in Bardeen’s model was attributed to the presence of a magnetic charge. Interestingly, subsequent work reinterpreted Bardeen’s solution as an NLED-driven GR solution, but with an electric charge as the source instead of a magnetic one [19].

Inspired by these groundbreaking contributions, numerous models of regular black holes have been proposed that incorporate NLED as the matter source in GR. Notable examples include the models developed by Bronnikov [20], Dymnikova [21], Balart and Vagenas [22], and Culetu [23]. These models have expanded the landscape of regular black hole solutions, offering new insights into their physical properties and implications. Simultaneously, the thermodynamic behavior of regular black holes has attracted significant attention, with studies examin-

ing their entropy, temperature, and stability under various conditions [24–28]. For a broader perspective on the applications and implications of regular black hole models within the framework of NLED and GR, we refer the reader to the works Balart, Kruglov, and Gullu, which delve into diverse scenarios and provide a comprehensive understanding of the subject [29–32]. These studies collectively highlight the relevance and versatility of NLED in addressing longstanding challenges in theoretical physics, particularly in the quest to resolve singularities in both gravitational and electromagnetic contexts.

Another notable development emerged in 1966, when Schwinger introduced the concept of a particle possessing both magnetic and electric charges [33]. This particle, now widely known as the dyon or dyonic solution, has since become a key element in theoretical physics. Dyonic solutions have been applied across a wide range of contexts, for instance, they have been employed in analyzing the properties of rotating black holes within the Tomimatsu-Sato-Yamazaki spacetime framework in the context of dyons [34]. They have also been used to study radiating massive objects [35], and their applications extend to string theory [36–43] and supergravity theories [44–49]. For readers interested in a deeper exploration of dyonic applications, we recommend consulting the extensive works available on the subject [50–65].

Indeed, in 2018, Simpson and Visser proposed a novel approach to address singularities in GR solutions through a framework now known as the Black Bounce (BB) model [66]. Motivated by regularizing parameters that eliminate the central singularity at $r = 0$, their proposal introduces a “bounce” structure mediated by one or more parameters related to a fundamental length scale. This regularization ensures that the spherical area radius remains non-zero, preventing the formation of a singularity and allowing for a smooth transition in the radial coordinate. The BB framework accommodates a variety of configurations, making it a powerful tool in gravitational physics. Among the notable solutions are regular black holes with symmetric horizons and a central bounce, one-way traversable wormholes, and two-way traversable wormholes. These configurations provide rich opportunities to explore spacetime geometries free from singularities, while also uncovering new physical phenomena. The BB framework has inspired the development of numerous extensions, alternative solutions, and analytical models, leading to significant advancements in the field. Research has focused on aspects such as the regularity of spacetime, causal structures, and energy conditions [67]; gravitational lensing effects [68–72]; and potential observational signatures [73–82]. Furthermore, generalizations of the BB model to rotating configurations have also been explored, extending its applicability to more realistic astrophysical scenarios [83, 84].

Black bounce (BB) configurations are typically obtained using an inverse method, wherein a predefined line element exhibiting bounce-like characteristics is first specified. The corresponding field equations are then

solved in reverse to identify the matter sources that give rise to the given spacetime geometry. In many cases, these material sources are described by a combination of NLED and scalar fields [85–88]. Historically, most BB solutions have used only a magnetic charge as the primary component of the Maxwell-Faraday tensor. More recently, however, BB solutions have been constructed using material sources with a purely electric charge embedded within the NLED structure [89]. This development opens the door to studying configurations that can exhibit both electric and magnetic charges, significantly broadening the scope of BB solutions and their applications. These developments highlight the ongoing refinement of the BB model and its potential to reveal novel insights into gravitational theory.

In this work, our primary objective is to investigate dyonic solutions within the framework of BB geometries in GR, incorporating both magnetic and electric charges in the structure of NLED, following the approach described by Bronnikov [20]. Specifically, we focus on static and spherically symmetric configurations, coupling NLED and a scalar field as matter sources in GR. Our analysis involves the development of BB solutions for various metric functions, where we numerically examine the existence and nature of horizons, assess the regularity of the solutions through the behavior of the Kretschmann scalar, and determine the material sources responsible for shaping the geometric structure of these configurations. Through this approach, we aim to provide a comprehensive understanding of dyonic BB solutions and their physical implications within this extended framework.

This work is organized as follows: In Sec. II, we provide a brief overview of the field equations for GR coupled with NLED and scalar fields, explicitly incorporating both magnetic and electric charges. In Secs. III to VI, we analyze and generalize various BB geometries, presenting several static and spherically symmetric solutions derived within this framework. Finally, in Sec. VII, we conclude by summarizing our results and discussing their implications.

II. FIELD EQUATIONS COUPLED TO NON-LINEAR SLECTRODYNAMICS AND SCALAR FIELD

A. Action and field equations

We begin our analysis with the following action:

$$S = \int \sqrt{-g} d^4x \left[R - 2\kappa^2 \left(\mathcal{L}(\varphi) - \mathcal{L}_{\text{NLED}}(F) \right) \right], \quad (1)$$

with $\kappa^2 = 8\pi$ and

$$\mathcal{L}(\varphi) = \epsilon \partial^\mu \varphi \partial_\mu \varphi - V(\varphi), \quad (2)$$

where $\epsilon = +1$ corresponds to a regular scalar field, while $\epsilon = -1$ represents a phantom scalar field. The field φ denotes the scalar field, while $V(\varphi)$ is the associated scalar

potential. Additionally, $\mathcal{L}_{\text{NLED}}(F)$ is the Lagrangian density that describes a NLED, which depends on the electromagnetic field scalar

$$F = \frac{1}{4} F^{\mu\nu} F_{\mu\nu}, \quad (3)$$

where the Maxwell-Faraday antisymmetric tensor is defined by

$$F_{\mu\nu} = \partial_\mu A_\nu - \partial_\nu A_\mu, \quad (4)$$

and A_μ is the magnetic vector potential.

Presented below are the equations of motion arising from the action (1):

$$\nabla_\mu (\mathcal{L}_F F^{\mu\nu}) = 0, \quad (5)$$

$$\nabla_\mu {}^*F^{\mu\nu} = 0, \quad (6)$$

$$2\epsilon \nabla_\mu \nabla^\mu \varphi = -\frac{dV(\varphi)}{d\varphi}, \quad (7)$$

where $\mathcal{L}_F = \partial \mathcal{L}_{\text{NLED}}(F) / \partial F$, ${}^*F^{\mu\nu} = \frac{1}{2\sqrt{-g}} \epsilon^{\mu\nu\alpha\beta} F_{\alpha\beta}$ and the asterisk denotes the Hodge dual ($*$).

The gravitational field equations are obtained by varying the action (1) with respect to the metric tensor, which yield:

$$G^\mu{}_\nu = R^\mu{}_\nu - \frac{1}{2} \delta^\mu{}_\nu R = \kappa^2 \left(\overset{F}{T}{}^\mu{}_\nu + \overset{\varphi}{T}{}^\mu{}_\nu \right). \quad (8)$$

Thus, the explicit form of the NLED energy-momentum tensor is expressed as follows

$$\overset{F}{T}{}^\mu{}_\nu = \frac{2}{\kappa^2} \left(\delta^\mu{}_\nu \mathcal{L}_{\text{NLED}}(F) - \mathcal{L}_F F^{\mu\alpha} F_{\nu\alpha} \right), \quad (9)$$

and the energy-momentum tensor for the scalar field matter part is defined as

$$\overset{\varphi}{T}{}^\mu{}_\nu = \epsilon \left(2 \partial^\mu \varphi \partial_\nu \varphi - \delta^\mu{}_\nu \partial^\sigma \varphi \partial_\sigma \varphi \right) + \delta^\mu{}_\nu V(\varphi). \quad (10)$$

In this work, we consider the following static and spherically symmetric metric to obtain our solutions:

$$ds^2 = A(r) dt^2 - \frac{1}{A(r)} dr^2 - \Sigma^2(r) d\Omega^2, \quad (11)$$

where $A(r)$ and $\Sigma(r)$ are functions of the radial coordinate r , and the two-sphere line element is defined as $d\Omega^2 \equiv d\theta^2 + \sin^2(\theta) d\phi^2$. Note that the metric function $\Sigma(r)$ allows us to express the metric in its most general form for spherical and static symmetry, as given in Eq. (11). In the sections that follow, we present the corresponding metrics for the solutions describing black holes and regular black holes.

Furthermore, we consider solutions described by the magnetic charge, q_m , and the electric charge q_e . The components of the $F_{\mu\nu}$ tensor are described by:

$$F_{01} = -F_{10} = \frac{q_e}{\Sigma^4(r) \mathcal{L}_F(r)}, \quad (12)$$

$$F_{23} = -F_{32} = q_m \sin \theta, \quad (13)$$

and the electromagnetic scalar takes the form

$$F = \frac{q_m^2 \mathcal{L}_F^2(r) - q_e^2}{2\mathcal{L}_F^2(r)\Sigma(r)^4}. \quad (14)$$

B. Strategy for solving the field equations

To assess the consistency of our solutions, we will also use the following relationship

$$\mathcal{L}_F = \frac{\partial \mathcal{L}_{\text{NLED}}}{\partial r} \left(\frac{\partial F}{\partial r} \right)^{-1}. \quad (15)$$

The components derived from the equations of motion, as described by Eq. (8), after substituting Eq. (11), are given by:

$$\begin{aligned} & \frac{\Sigma(r) (A'(r)\Sigma'(r) + 2A(r)\Sigma''(r)) + A(r)\Sigma'(r)^2 - 1}{\Sigma(r)^2} \\ &= \kappa^2 \left(\epsilon A(r)\varphi'(r)^2 + V(r) \right) \\ &+ 2 \left(\mathcal{L}_{\text{NLED}}(r) + \frac{q_e^2}{\mathcal{L}_F(r)\Sigma(r)^4} \right), \end{aligned} \quad (16)$$

$$\begin{aligned} \mathcal{L}_{\text{NLED}}(r) = & \frac{1}{8\Sigma(r)^4} \left\{ -\Sigma(r)^4 \left[A''(r) + 4\kappa^2 \left(\epsilon A(r)\varphi'(r)^2 + V(r) \right) \right] - 2\Sigma(r)^3 (2A'(r)\Sigma'(r) + 3A(r)\Sigma''(r)) \right. \\ & \left. - 2\Sigma(r)^2 (A(r)\Sigma'(r)^2 - 1) + \sqrt{\Sigma(r)^4 \left[\Sigma(r)^2 A''(r) - 2A(r) \left(\Sigma(r)\Sigma''(r) + \Sigma'(r)^2 \right) + 2 \right]^2 - 64q_e^2 q_m^2} \right\}, \end{aligned} \quad (19)$$

and

$$\begin{aligned} \mathcal{L}_F(r) = & \frac{1}{8q_m^2} \left\{ \Sigma(r)^4 A''(r) - 2A(r)\Sigma(r)^3 \Sigma''(r) - 2\Sigma(r)^2 (A(r)\Sigma'(r)^2 - 1) \right. \\ & \left. + \sqrt{\Sigma(r)^4 \left[\Sigma(r)^2 A''(r) - 2A(r) \left(\Sigma(r)\Sigma''(r) + \Sigma'(r)^2 \right) + 2 \right]^2 - 64q_e^2 q_m^2} \right\}. \end{aligned} \quad (20)$$

If we now insert Eqs. (19) and (20) into the equation of motion (17), we get

$$\frac{2A(r) (\Sigma''(r) + \kappa^2 \epsilon \Sigma(r)\varphi'(r)^2)}{\Sigma(r)} = 0. \quad (21)$$

Thus, as stated above, Eq. (21) can be solved to determine the general form of the scalar field $\varphi(r)$, whose explicit expression is presented below

$$\varphi(r) = \int \frac{\sqrt{\Sigma''(r)}}{\kappa \sqrt{(-\epsilon)\Sigma(r)}} dr. \quad (22)$$

With this scalar field, the potential $V(r)$ can now be determined after solving Eq. (7), which yields the follow-

$$\begin{aligned} & \frac{\Sigma(r)A'(r)\Sigma'(r) + A(r)\Sigma'(r)^2 - 1}{\Sigma(r)^2} \\ &= \kappa^2 \left(V(r) - \epsilon A(r)\varphi'(r)^2 \right) \\ &+ 2 \left(\mathcal{L}_{\text{NLED}}(r) + \frac{q_e^2}{\mathcal{L}_F(r)\Sigma(r)^4} \right), \end{aligned} \quad (17)$$

$$\begin{aligned} & \frac{\Sigma(r)A''(r) + 2A'(r)\Sigma'(r) + 2A(r)\Sigma''(r)}{2\Sigma(r)} \\ &= \kappa^2 \left(\epsilon A(r)\varphi'(r)^2 + V(r) \right) \\ &+ 2 \left(\mathcal{L}_{\text{NLED}}(r) - \frac{q_m^2 \mathcal{L}_F(r)}{\Sigma(r)^4} \right). \end{aligned} \quad (18)$$

We can solve the set of equations (16)–(18) using two different approaches. In the first approach, we derive the general expressions for $\mathcal{L}_{\text{NLED}}(r)$ and $\mathcal{L}_F(r)$ from the equations of motion (16) and (18). This process ensures that only the equation of motion (17) remains, which we then use to determine the scalar field $\varphi(r)$. Following this strategy, we obtain the following quantities directly from the equations of motion (16) and (18):

ing:

$$\begin{aligned} V(r) = & \int \frac{1}{\Sigma(r)^2} \left[\Sigma''(r) \left(2\Sigma(r)A'(r) + 3A(r)\Sigma'(r) \right) \right. \\ & \left. + A(r)\Sigma(r)\Sigma'''(r) \right] dr. \end{aligned} \quad (23)$$

The second strategy follows an analogous approach to the first. However, in this case, we use the equations of motion (17) and (18) to determine the general forms of $\mathcal{L}_{\text{NLED}}(r)$ and $\mathcal{L}_F(r)$. These expressions can then be substituted into the equation of motion (16) to obtain the same scalar field $\varphi(r)$ given by (22), and consequently, the same potential as in (23). Thus, we conclude that the solutions obtained using the second strategy for $A(r)$, $\Sigma(r)$, $\mathcal{L}_{\text{NLED}}(r)$, $\mathcal{L}_F(r)$, $\varphi(r)$, and $V(r)$ are identical to those obtained with the first approach.

To analyze the properties of the metric functions, which will be presented later, and to determine the presence of horizons, we impose the following condition:

$$A(r_H) = 0, \quad (24)$$

where the radius r_H denotes the radial coordinate of the horizon. Moreover, a second condition allows one to compute the number of horizons of a given metric function

$$\left. \frac{dA(r_H)}{dr} \right|_{r=r_H} = 0. \quad (25)$$

These two relations allow us to identify degenerate horizons and subsequently determine the critical values of the parameters for each model (i.e. mass M , electric charge q_e , or magnetic charge q_m), which will be obtained in the following sections. To achieve this, we will numerically solve Eqs. (24) and (25) simultaneously to obtain the critical value of one of the geometry's free parameters, while fixing the values of the other two. This is done for all three possible free parameters. In this way, we will analyze additional solutions based on the chosen parameter values, thus exploring the available range of geometric structures.

Additionally, we will calculate the Komar mass for our models [90]. This quantity is essential for determining the mass of a stationary, asymptotically flat spacetime and is directly related to the Killing field. The Komar mass is determined by the following surface integral

$$\bar{M}_K = -\frac{1}{8\pi} \int_{\infty} \star dk, \quad (26)$$

where $k = g_{tt}dt$ is the covector associated with the Killing field asymptotically similar to the time field ∂_t .

For a metric that depends only on the radial coordinate r , as is the case discussed in this manuscript and illustrated by the metric (11), we can simplify the integral (26) as follows

$$M_K = \lim_{r \rightarrow \infty} \frac{1}{2} r^2 \partial_r A(r). \quad (27)$$

We shall use Eq. (27) to calculate the Komar mass in our models.

C. Dyonic Reissner-Nordström type solution

As an example, and a first solution, we assume that the contribution of the scalar field is zero, i.e. $V(r) = 0$ and $\varphi(r) = 0$. We also assume that $\Sigma(r) = r$ and that the Lagrangian and its derivative are

$$\mathcal{L}_{\text{NLED}}(r) = F, \quad (28)$$

$$\mathcal{L}_F(r) = 1. \quad (29)$$

With these assumptions, we obtain the following equations of motion:

$$-\frac{rA'(r) + A(r) - 1}{r^2} = \frac{q_e^2 + q_m^2}{r^4}, \quad (30)$$

$$\frac{A''(r)}{2} = \frac{r^3(-A'(r)) + q_e^2 + q_m^2}{r^4}, \quad (31)$$

which provide us with the following solution

$$A(r) = 1 - \frac{2M}{r} + \frac{q_e^2 + q_m^2}{r^2}. \quad (32)$$

This metric function satisfies all equations of motion and is known as the dyonic Reissner-Nordström solution. If we consider the magnetic charge to be zero ($q_m = 0$), we obtain the Reissner-Nordström metric function.

The Komar mass for this model, given by Eq. (27), is:

$$M_K = \lim_{r \rightarrow \infty} \left(M - \frac{(q_e^2 + q_m^2)}{r} \right) = M. \quad (33)$$

Thus, the parameter M , described by Eq. (32), is identical to the Komar mass given by Eq. (33).

III. DYON SOLUTIONS OF THE SIMPSON-VISSER TYPE

In this model, we generalize the Simpson-Visser model by incorporating both the magnetic charge q_m and the electric charge q_e . However, due to the direct algebraic construction employed in deriving this solution, certain inconsistencies may arise. For instance, the Lagrangian $\mathcal{L}(r)$ and its derivative $\mathcal{L}_F(r)$ are not real over the entire range of the radial coordinate r . We will further discuss these results in the following sections.

A. Dyon solutions of the Simpson-Visser type

In this approach, we extend the metric function of the Simpson-Visser BB model to the dyonic framework to derive our solutions. In this process, we consider that

$$A(r) = 1 - \frac{2M}{\sqrt{q_e^2 + q_m^2 + r^2}}. \quad (34)$$

Setting the electrical charge $q_e = 0$ in Eq. (34), yields the Simpson-Visser solution.

With the purpose of generating a bounce, we can choose the canonical form of the area function described as follows,

$$\Sigma(r) = \sqrt{q_m^2 + r^2}, \quad (35)$$

where the coordinate r ranges over $(-\infty, +\infty)$, while the function $\Sigma(r)$, which defines the areal radius of the two-spheres, is given by $S = 4\pi\Sigma^2(r)$ and assumes a minimum value of $\Sigma(r) = q_m$ at $r = 0$.

As we develop dyon solutions in this manuscript we will conveniently consider an appropriate generalization of the function described by Eq. (35). Namely, we will adopt the following form

$$\Sigma(r) = \sqrt{q_e^2 + q_m^2 + r^2}. \quad (36)$$

With this definition, the minimum value of Eq. (36) occurs when $\Sigma(0) = \sqrt{q_e^2 + q_m^2}$, and we recover the Simpson-Visser area function, when we set $q_e = 0$ in Eq. (36).

Now, we simultaneously solve Eqs. (24) and (25) to determine the critical electric charge, which is $q_{ec} = 19.999$ when we assign the constant values $M = 10.0$ and $q_m = 0.2$. In the left plot of Fig. 1, we illustrate the behavior of the metric function (34) with respect to the radial coordinate r for three different scenarios of the electric charge: $q_e > q_{ec}$, $q_e = q_{ec}$ and $q_e < q_{ec}$.

Similarly, by simultaneously solving Eqs. (24) and (25), we find the critical magnetic charge $q_{mc} = 9.797$ when we choose the constant values $M = 5.0$ and $q_e = 2.0$. We illustrate the behavior of the metric function (34) for this case in the right plot of Fig. 1 considering the scenarios of magnetic charge: $q_m > q_{mc}$, $q_m = q_{mc}$ and $q_m < q_{mc}$. We observe a similar behavior in all three scenarios, when varying the corresponding free parameter, as illustrated in Figs. 1 and 2.

The critical mass M_c , determined by solving Eqs. (24) and (25) simultaneously, is found to be $M_c = 0.395$ when we choose the constant values as $q_e = 0.25$ and $q_m = 0.75$. Fig. 2 shows the behavior of the metric function (34) in terms of the radial coordinate r , for three mass scenarios: $M > M_c$, $M = M_c$, and $M < M_c$.

Using Eq. (27) we computed the Komar mass, for the metric function (34). In this case, we obtained:

$$M_K = \lim_{r \rightarrow \infty} \frac{Mr^3}{(q_e^2 + q_m^2 + r^2)^{3/2}} = M. \quad (37)$$

Thus, the parameter M , described by Eq. (34), is identical to the Komar mass given by Eq. (37).

B. Kretschmann scalar

On the other hand, we can study the regularity properties of our model by computing the Kretschmann scalar, which for the present case is given by

$$K(r) = \frac{4}{(q_e^2 + q_m^2 + r^2)^5} \left\{ 3(q_e^2 + q_m^2)^2 (q_e^2 + q_m^2 + r^2) - 8M(q_e^2 + q_m^2)(q_e^2 + q_m^2 - r^2) \sqrt{q_e^2 + q_m^2 + r^2} + 3M^2 \left[-4r^2(q_e^2 + q_m^2) + 3(q_e^2 + q_m^2)^2 + 4r^4 \right] \right\}. \quad (38)$$

Note that the Kretschmann scalar is regular for small values of r , i.e. in the limit $r \rightarrow 0$

$$\lim_{r \rightarrow 0} K(r) = \frac{4(9M^2 - 8M\sqrt{q_e^2 + q_m^2} + 3q_e^2 + 3q_m^2)}{(q_e^2 + q_m^2)^3}. \quad (39)$$

We observe that the Kretschmann scalar is asymptotically flat for very large values of r , i.e. in the limit $r \rightarrow \infty$. We illustrate the behavior of the Kretschmann scalar for this model in Fig. 3.

C. Matter Lagrangian and Potential reconstruction

By considering the model described by Eq. (36) and substituting it into the scalar field equation (22), we obtain $\varphi(r)$, which will be used in the subsequent models discussed below:

$$\varphi(r) = \frac{\tan^{-1} \left(\frac{r}{\sqrt{q_e^2 + q_m^2}} \right)}{\sqrt{\kappa^2(-\epsilon)}}. \quad (40)$$

Note that if we consider zero electric charge in the scalar field above, Eq. (40), we recover the scalar field obtained in the work of [87].

By substituting the model (36) and the metric function (34) into Eq. (23), we obtain the expression for the potential as a function of the radial coordinate:

$$V(r) = \frac{4M(q_e^2 + q_m^2)}{5\kappa^2(q_e^2 + q_m^2 + r^2)^{5/2}}. \quad (41)$$

With the quantities such as the function (36), the metric function (34), the scalar field (40) and the potential (41), we can explicitly express the Lagrangian $\mathcal{L}_{\text{NLED}}$ for this model, which is derived from the general Lagrangian given by Eq. (19), as

$$\mathcal{L}_{\text{NLED}}(r) = \frac{\sqrt{\frac{9M^2(q_e^2 + q_m^2)^2}{q_e^2 + q_m^2 + r^2} - 16q_e^2 q_m^2}}{4(q_e^2 + q_m^2 + r^2)^2} - \frac{3M(q_e^2 + q_m^2)}{20(q_e^2 + q_m^2 + r^2)^{5/2}}, \quad (42)$$

and its derivative \mathcal{L}_F as

$$\mathcal{L}_F(r) = \frac{\sqrt{\frac{9M^2(q_e^2 + q_m^2)^2}{q_e^2 + q_m^2 + r^2} - 16q_e^2 q_m^2} + \frac{3M(q_e^2 + q_m^2)}{\sqrt{q_e^2 + q_m^2 + r^2}}}{4q_m^2}. \quad (43)$$

With the metric function (34), the function (36), the scalar field (40), the potential (41), the Lagrangian (42), and its derivative (43), we now satisfy all equations (5)–(7) and (15), as well as all components of the equations of motion (16)–(18).

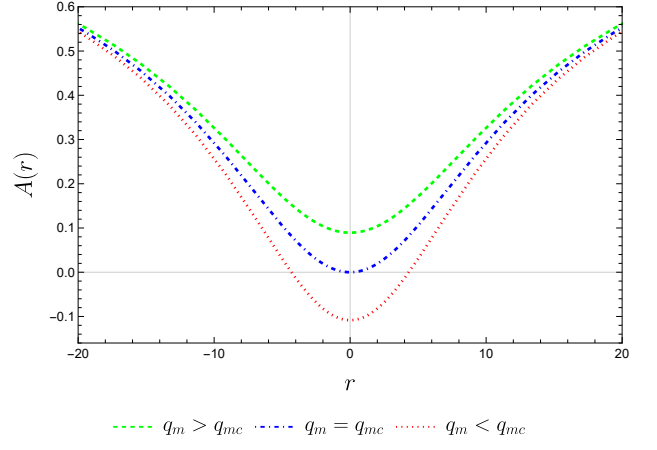
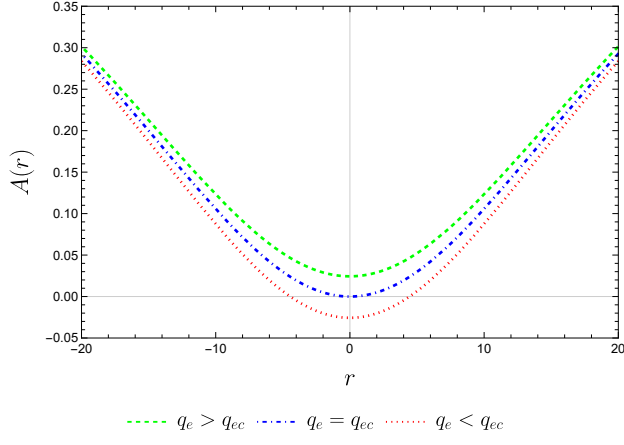


Figure 1. The metric function $A(r)$, given by Eq. (34). (i) The left plot depicts three electric charge scenarios, where we have used the values of the constants as follows $\{M = 10.0$ and $q_m = 0.2$. (ii) The right plot depicts three magnetic charge scenarios, with the following values $M = 5.0$ and $q_e = 2.0$.

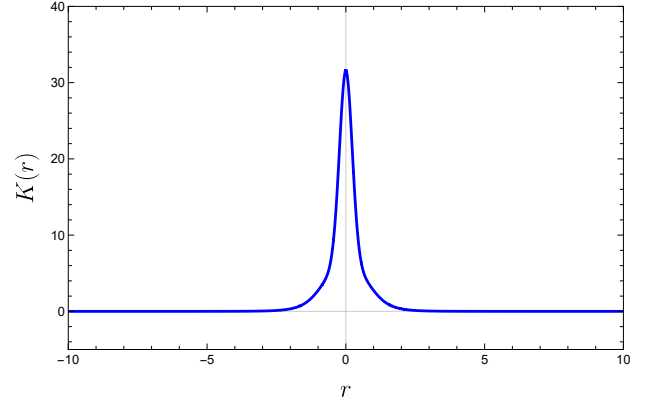
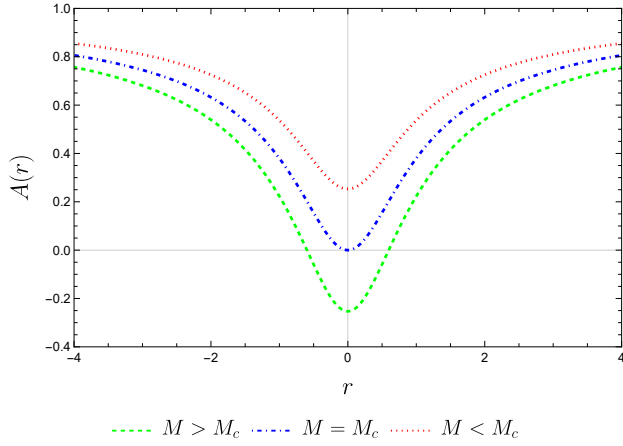


Figure 2. The metric function $A(r)$, given by Eq. (34) for three mass scenarios. We have used the values of the constants as follows $\{q_e = 0.25$, and $q_m = 0.75\}$

Figure 3. The scalar of Kretschmann $K(r)$, given by Eq. (38). We have used the values of the constants as follows $\{M = 1.0$, $q_e = 0.5$, $q_m = 0.75\}$.

Now the electromagnetic scalar (3) for this solution has the form of:

$$\begin{aligned}
 F(r) = & q_m^2 \left[(q_e^2 + q_m^2) \left(\frac{9M^2 (q_e^2 + q_m^2)^2}{q_e^2 + q_m^2 + r^2} - 16q_e^2 q_m^2 \right) \right]^{\frac{1}{2}} \\
 & \times 3M \sqrt{q_e^2 + q_m^2 + r^2} - 16q_e^2 q_m^2 (q_e^2 + q_m^2 + r^2) \\
 & + 9M^2 (q_e^2 + q_m^2)^2 \Big] / (q_e^2 + q_m^2 + r^2)^2 \left[3M (q_e^2 + q_m^2) \right. \\
 & \left. + \sqrt{q_e^2 + q_m^2 + r^2} \sqrt{\frac{9M^2 (q_e^2 + q_m^2)^2}{q_e^2 + q_m^2 + r^2} - 16q_e^2 q_m^2} \right]^2. \quad (44)
 \end{aligned}$$

Note that we recover the electromagnetic scalar of the Simpson-Visser solution by taking $q_e = 0$ in Eq. (44). We highlight the behavior of the electromagnetic scalar (44) in two distinct scenarios.

In the first scenario, we present three curves for different values of the electric charge ($q_e = 0.25$, $q_e = 0.5$ and $q_e = 0.75$), as illustrated in the left plot of Fig. 4. In the second scenario, we highlight the behavior of this scalar when varying the magnetic charge for three different curves with ($q_m = 0.25$, $q_m = 0.5$ and $q_m = 0.75$), as shown in the right plot of Fig. 4. We observe in the left plot of Fig. 4 that as the electric charge varies, the amplitude decreases, while in the right plot of Fig. 4, the amplitude is greater when $q_e = q_m$.

By inverting the expression (40), we obtain $r(\varphi)$ and determine

$$V(\varphi) = \frac{4M (q_e^2 + q_m^2)}{5\kappa^2 \left[(q_e^2 + q_m^2) \operatorname{sech}^2(\kappa\varphi\sqrt{\epsilon}) \right]^{5/2}}. \quad (45)$$

If we take $q_e = 0$ in this potential, we recover the potential obtained in [87].

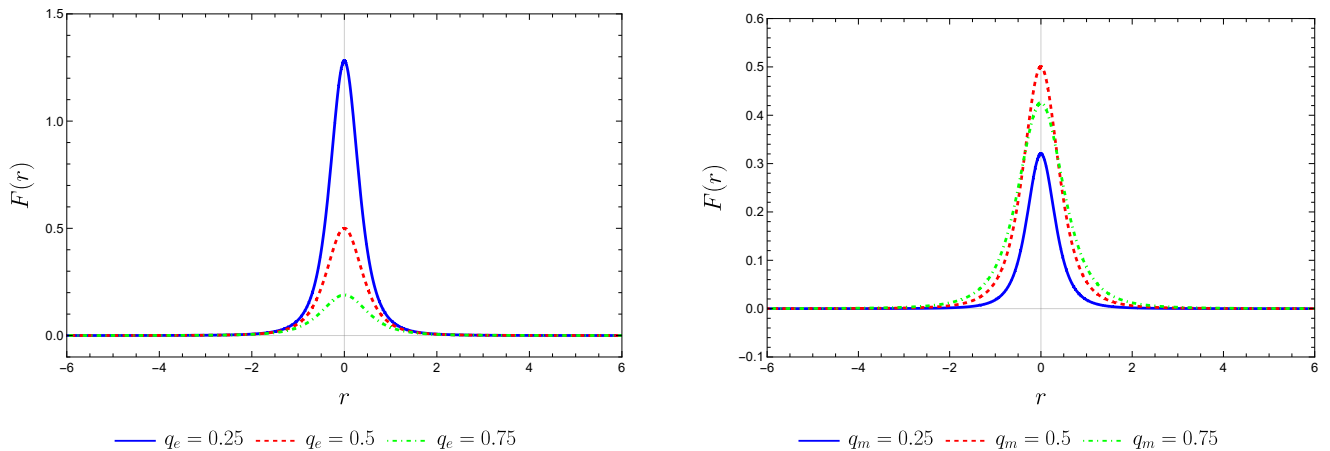


Figure 4. The electromagnetic scalar F , given by Eq. (44). (i) The left plot depicts different values of the electric charge, where we have used the following values $\{M = 10.0, q_m = 0.75\}$. In the right plot, we have varied the values of the magnetic charge, and considered the values of the constants as follows $\{M = 10.0, q_e = 0.5\}$.

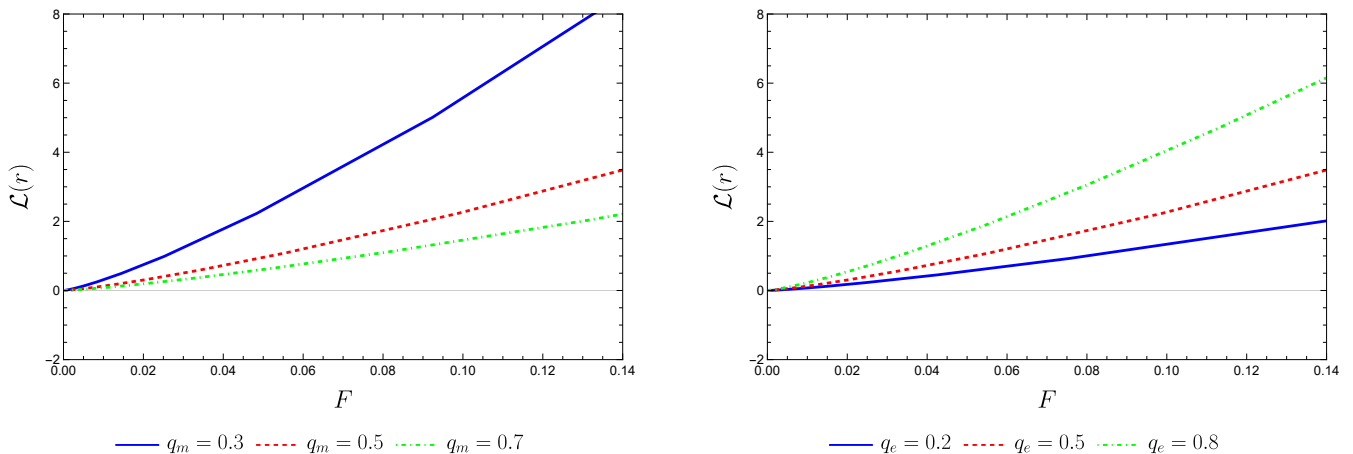


Figure 5. The NLED Lagrangian $\mathcal{L}(F)$, for different values of the electric charge and the magnetic charge. (i) In the left plot, we use the values of the constants as follows $\{M = 10.0, q_e = 0.5\}$. (ii) In the right plot, we consider $\{M = 10.0, q_m = 0.5\}$.

In the plots of Fig. 5 we show the behavior of the Lagrangian density of NLED as a function of F using a parametric plot, for different values of the electric charge and of the magnetic charge. We also illustrate the behavior of the scalar field potential given by Eq. (45) in three distinct plots, each showing three curves with variations of electric charge, magnetic charge and mass values, as detailed in Figs. 6 and 7. We notice that the amplitude of the potential also varies as we change the values for the electric charge, magnetic charge and mass.

IV. THIRD DYON SOLUTION.

A. Metric function and horizons

In Eq. (19), to ensure that the Lagrangian $\mathcal{L}_{\text{NLED}}(r)$ remains real, the expression inside the square root in

Eq. (19) must always be a positive real number. To satisfy this condition, we impose the following requirement:

$$\begin{aligned} [\Sigma(r)^2 A''(r) - 2A(r) (\Sigma(r)\Sigma''(r) + \Sigma'(r)^2) + 2]^2 = \\ = 64q_e^2 q_m^2. \end{aligned} \quad (46)$$

By considering the function (36), we simplify the previous expression as

$$[A''(r) (q_e^2 + q_m^2 + r^2) - 2A(r) + 2]^2 = 64q_e^2 q_m^2, \quad (47)$$

which yields the following metric function

$$\begin{aligned} A(r) = 1 - 4\sqrt{q_e^2 q_m^2} + c_1 (q_e^2 + q_m^2 + r^2) + \frac{c_2 r}{2(q_e^2 + q_m^2)} \\ + \frac{c_2 (q_e^2 + q_m^2 + r^2)}{2(q_e^2 + q_m^2)^{3/2}} \tan^{-1} \left(\frac{r}{\sqrt{q_e^2 + q_m^2}} \right). \end{aligned} \quad (48)$$

The integration constants c_1 and c_2 are related to the gravitational mass or the gravitational energy of the sys-

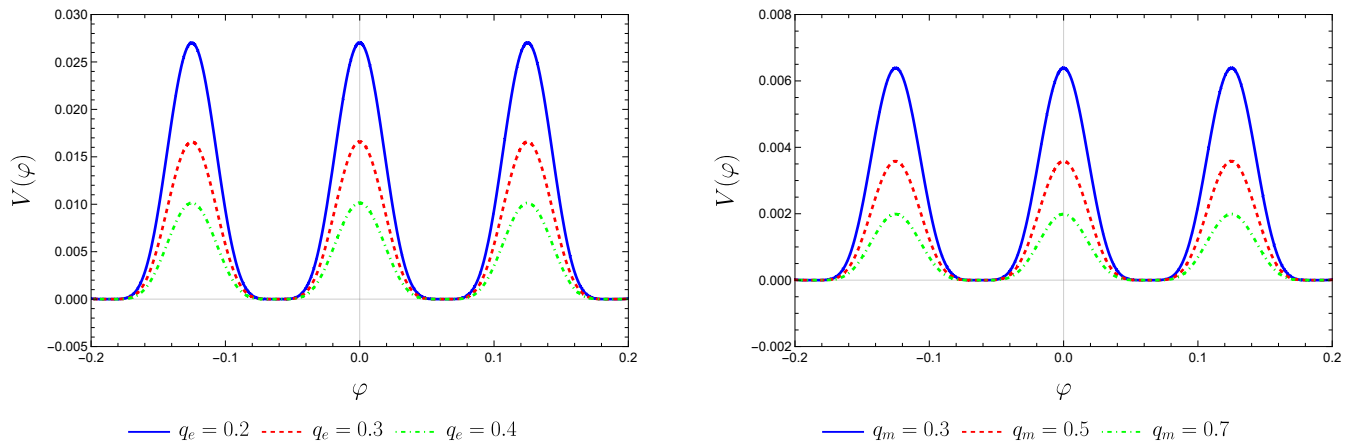


Figure 6. The scalar field potential $V(\varphi)$, described by Eq. (45) for different values of the electric charge and the magnetic charge, taking $\epsilon = -1$. (i) The left plot depicts the values of the constants $\{M = 1.0, q_m = 0.3\}$. (ii) The right plot represents the values for $\{M = 1.0, q_e = 0.5\}$.

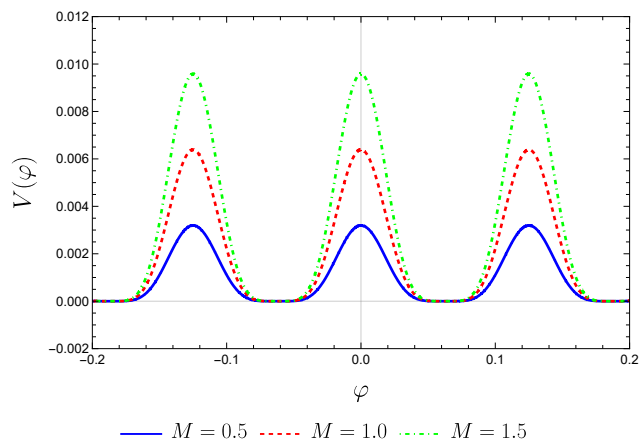


Figure 7. The scalar field potential $V(\varphi)$, described by Eq. (45) for different values of the mass, taking $\epsilon = -1$, for the values of the constants $\{q_e = 0.3, q_m = 0.5\}$.

tem. We will discuss this relationship in more detail when we calculate the Komar mass for this model.

In this case, we solve Eqs. (24) and (25) simultaneously to determine the critical electric charge, which for this solution is $q_{ec} = 0.681$ when the constants are assigned the values $q_m = 2.0$, $c_1 = 1$ and $c_2 = 1$. In the left plot of Fig. 8 we show the behavior of the metric function (48) with respect to the radial coordinate r for three different scenarios of the electric charge: $q_e > q_{ec}$, $q_e = q_{ec}$ and $q_e < q_{ec}$. If the electric charge is greater than the critical value $q_e > q_{ec}$, no horizon is formed, which leads to a wormhole geometry with a traversable throat at $r = 0$. When the electric charge is equal to the critical value $q_e = q_{ec}$, we observe a degenerate double horizon at $r = 0$, with a bounce still present at $r = 0$. Finally, when the electric charge is smaller than the critical electric charge, $q_e < q_{ec}$, we observe the presence of two event

horizons. At $r = 0$, a bounce occurs, allowing a transition between the regions $r > 0$ and $r < 0$, and vice versa, due to the symmetry with respect to r . Furthermore, we observe that varying the values of the solution parameters enhances the asymmetrical nature of the metric function (48).

We used the same procedure developed earlier to calculate q_{ec} , but now to determine the critical magnetic charge. We found that $q_{mc} = 2.093$ when the values of the constants are $q_e = 0.7$, $c_1 = 1$, and $c_2 = 1$. In the right plot of Fig. 8, we show the behavior of the metric function (48) with respect to the radial coordinate r for three different scenarios of the magnetic charge: $q_m > q_{mc}$, $q_m = q_{mc}$, and $q_m < q_{mc}$.

In general, the solution given by Eq. (48) is not asymptotically flat, which complicates the definition of the mass M or the gravitational energy. However, this limitation can be overcome by making an appropriate choice of constants to render the metric function (48) asymptotically flat, thus allowing for an accurate determination of the mass or gravitational energy of the system. To achieve this goal, we define the constant c_2 as

$$c_2 = -\frac{4c_1 (q_e^2 + q_m^2)^{3/2}}{\pi}. \quad (49)$$

With this choice, the metric function of the model becomes asymptotically flat. After substituting the constant c_2 , the metric function (48) can now be rewritten as

$$A(r) = 1 + c_1 \left(r^2 + q_e^2 + q_m^2 - \frac{2r\sqrt{q_e^2 + q_m^2}}{\pi} \right) - 4\sqrt{q_e^2 + q_m^2} - \frac{2c_1}{\pi} (q_e^2 + q_m^2 + r^2) \tan^{-1} \left(\frac{r}{\sqrt{q_e^2 + q_m^2}} \right). \quad (50)$$

We also determine the Komar mass, as given by Eq. (27), for the metric function described by Eq. (50),

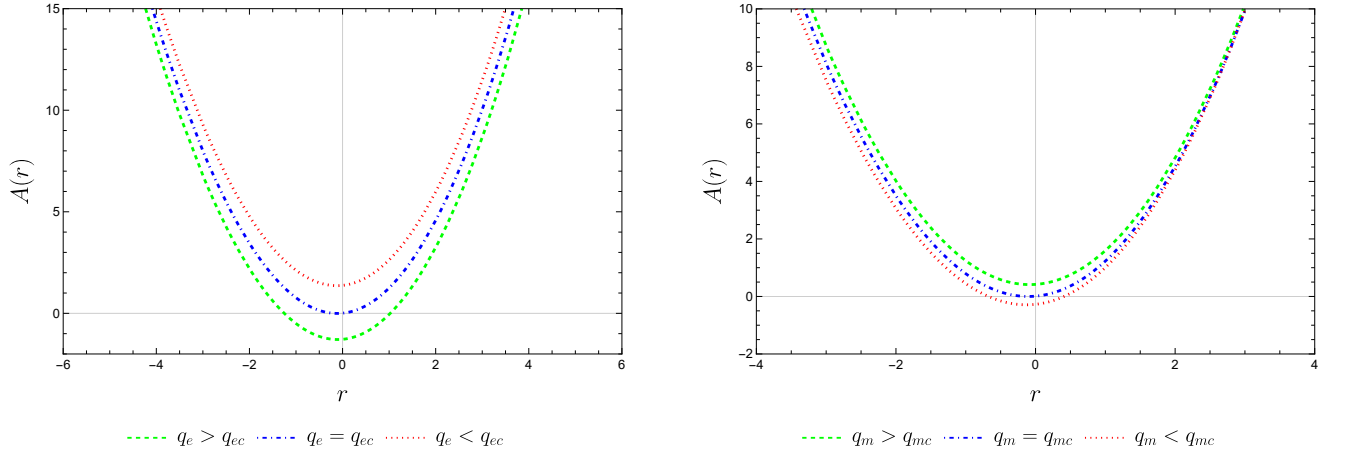


Figure 8. The metric function $A(r)$, given by Eq. (48) for electric charge and magnetic charge scenarios. (i) In the left plot, we have used the values of the constants as follows $\{q_m = 2.0, c_1 = 1.0, c_2 = 1.0\}$. (ii) In the right plot, we have considered the following values $\{q_m = 0.7, c_1 = 1.0, c_2 = 1.0\}$.

which for this model is given by:

$$M_K = \frac{2\bar{c}_1}{3\pi}, \quad (51)$$

where we replace $c_1 = -\bar{c}_1 (q_e^2 + q_m^2)^{-3/2}$, and \bar{c}_1 is a new positive real numerical constant that is independent of the electric and magnetic charges, ensuring that the Komar mass is also independent.

Instead of assuming a constant c_2 , it is also possible to adopt the constant c_1 . In this way, we now consider

$$c_1 = -\frac{\pi c_2}{4 (q_e^2 + q_m^2)^{3/2}}, \quad (52)$$

so that the metric function (48) becomes asymptotically flat. Substituting this constant c_1 into the metric function (48), we obtain:

$$A(r) = 1 - \frac{\pi c_2 (q_e^2 + q_m^2 + r^2)}{4 (q_e^2 + q_m^2)^{3/2}} + \frac{c_2 r}{2 (q_e^2 + q_m^2)} - 4\sqrt{q_e^2 q_m^2} + \frac{c_2 (q_e^2 + q_m^2 + r^2)}{2 (q_e^2 + q_m^2)^{3/2}} \tan^{-1} \left(\frac{r}{\sqrt{q_e^2 + q_m^2}} \right). \quad (53)$$

In this manner, we determine the Komar mass, as given by Eq. (27), for the metric function (53). Its explicit form is now

$$M_K = \frac{c_2}{6}. \quad (54)$$

B. Kretschmann and electromagnetic scalar

In order to gain a better understanding of the regularity properties of our model, we calculate the Kretschmann scalar for this solution. Taking the limit

of $r \rightarrow 0$ for the Kretschmann scalar, we observe that it is regular under this condition

$$\lim_{r \rightarrow 0} K(r) = 4 \left[3c_1^2 (q_e^2 + q_m^2)^2 + 32q_e^2 q_m^2 - 16\sqrt{q_e^2 q_m^2} - 4c_1 (q_e^2 + q_m^2) \left(4\sqrt{q_e^2 q_m^2} - 1 \right) + 3 \right] / (q_e^2 + q_m^2)^2. \quad (55)$$

We also observe that the Kretschmann scalar is regular for very large values of r

$$\lim_{r \rightarrow \infty} K(r) = \frac{3 \left(4c_1 (q_e^2 + q_m^2) + \pi c_2 \sqrt{\frac{1}{q_e^2 + q_m^2}} \right)^2}{2 (q_e^2 + q_m^2)^2}. \quad (56)$$

The Kretschmann scalar expression for this model is quite complicated, therefore, we illustrate its regular behavior as depicted in Fig. 9.

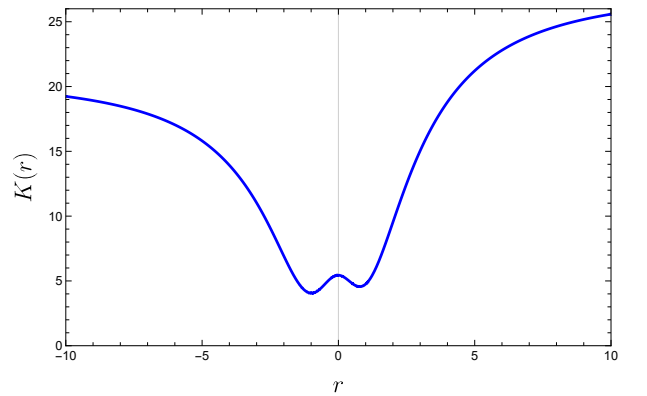


Figure 9. The behavior of the Kretschmann scalar $K(r)$. We have used the values of the constants as follows $\{q_e = 1.0, q_m = 2.0, c_1 = 1.0, c_2 = 1.0\}$.

C. Matter Lagrangian and Potential

Substituting Eq. (36) and the metric function (48) into Eq. (23), we obtain the form of the potential as a function of the radial coordinate:

$$V(r) = -\frac{3c_2 r - 4c_1 (q_e^2 + q_m^2)^2}{2\kappa^2 (q_e^2 + q_m^2) (q_e^2 + q_m^2 + r^2)} - \frac{c_2 (q_e^2 + q_m^2 + 3r^2) \tan^{-1}\left(\frac{r}{\sqrt{q_e^2 + q_m^2}}\right)}{2\kappa^2 (q_e^2 + q_m^2)^{3/2} (q_e^2 + q_m^2 + r^2)}. \quad (57)$$

Having used the appropriate quantities such as the function (36), the metric function (48), the scalar field (40) and the potential (57), we can explicitly express the Lagrangian $\mathcal{L}_{\text{NLED}}$ for this model, which is derived from the general Lagrangian given by Eq. (19),

$$\mathcal{L}_{\text{NLED}}(r) = -\frac{3c_1}{2} + \frac{\sqrt{q_e^2 q_m^2}}{(q_e^2 + q_m^2 + r^2)^2} \left[(q_e^2 + q_m^2 + r^2) + \sqrt{(q_e^2 + q_m^2 + r^2 - 1)(q_e^2 + q_m^2 + r^2 + 1)} \right], \quad (58)$$

whose derivative \mathcal{L}_F , Eq. (20), is given by

$$\mathcal{L}_F(r) = \frac{\sqrt{q_e^2 q_m^2}}{q_m^2} \left[(q_e^2 + q_m^2 + r^2) + \sqrt{(q_e^2 + q_m^2 + r^2 - 1)(q_e^2 + q_m^2 + r^2 + 1)} \right]. \quad (59)$$

Now, with the function (36), the metric function (48), the scalar field (40), the potential (57), the Lagrangian (58), and the derivative of the Lagrangian (59), we can satisfy all equations (5)–(7) and (15), as well as all components of the equations of motion (16)–(18).

We note that for small values of r the Lagrangian (58) and the derivative (59) are pure imaginary if $q_e^2 + q_m^2 \ll 1$.

In turn, from Eq. (14), we determined that the electromagnetic scalar for this solution has the following form:

$$F(r) = \frac{1}{q_e^2 + q_m^2 + r^2} - \frac{q_e^2 + r^2}{(q_e^2 + q_m^2 + r^2)^2} - q_m^2 + \frac{q_m^2 \sqrt{(q_e^2 + q_m^2 + r^2 - 1)(q_e^2 + q_m^2 + r^2 + 1)}}{(q_e^2 + q_m^2 + r^2)}. \quad (60)$$

Once more, we describe the behavior of the electromagnetic scalar (60) in two different scenarios. First, we present three curves for different values of electric charge ($q_e = 1.0$, $q_e = 2.0$ and $q_e = 3.0$), as shown in the left plot of Fig. 10. Secondly, we illustrate the behavior of this scalar when varying the magnetic charge for three different curves with ($q_m = 1.0$, $q_m = 2.0$ and $q_m = 3.0$), as shown in the right plot of Fig. 10.

By inverting Eqs. (40) and (60), we rewrite $r(\varphi)$ and $r(F)$ respectively. In this way, we express the Lagrangian

in terms of F in the form

$$\mathcal{L}_{\text{NLED}}(F) = -\frac{3c_1}{2} + \frac{(2Fq_m^2 - \sqrt{q_m^8 - 4Fq_m^6 + q_m^4})}{2q_m^4} \times \sqrt{q_e^2 q_m^2} \left[\sqrt{\frac{2q_m^4}{2Fq_m^2 - \sqrt{q_m^8 - 4Fq_m^6 + q_m^4}}} + \sqrt{\frac{(-2Fq_m^2 + \sqrt{q_m^8 - 4Fq_m^6 + q_m^4})}{2Fq_m^2 - \sqrt{q_m^8 - 4Fq_m^6 + q_m^4}}} \right], \quad (61)$$

and the potential in terms of the scalar field as

$$V(\varphi) = \frac{c_2 \tan^{-1}[\tan(\varphi\sqrt{\kappa^2(-\epsilon)})]}{2\kappa^2 (q_e^2 + q_m^2)^{3/2}} [\cosh(2\kappa\varphi\sqrt{\epsilon}) - 2] + \frac{\cosh^2(\kappa\varphi\sqrt{\epsilon}) [4c_1 (q_e^2 + q_m^2)^{3/2} - 3c_2 \tan(\varphi\sqrt{\kappa^2(-\epsilon)})]}{2\kappa^2 (q_e^2 + q_m^2)^{3/2}}. \quad (62)$$

In Fig. 11 we show the behavior of the Lagrangian density $\mathcal{L}_{\text{NLED}}$ as a function of F , for different values of the electric charge. We also illustrate the behavior of the scalar field potential given by Eq. (62) in distinct plots, each showing three curves with variations of electric charge and magnetic charge, as detailed in Figs. 12. We notice that the amplitude of the potential also varies as we change the values for electric charge, magnetic charge and mass.

Additionally, we observe that for very small values of F we get

$$\mathcal{L}_{\text{NLED}}(F) \sim -\frac{3c_1}{2} + \frac{2\sqrt{F}}{q_m^2} \left(\frac{\sqrt{q_e^2 q_m^4}}{\sqrt{2}} + \frac{\sqrt{q_m^2} \sqrt{q_e^2 q_m^2}}{\sqrt{2}} \right). \quad (63)$$

V. FOURTH DYON SOLUTION

A. Metric function and horizons

In this section, we consider the function described by (36) and a generalization of the metric function (48) described by:

$$A(r) = 1 - \frac{2M}{\sqrt{q_e^2 + q_m^2 + r^2}} - 4\sqrt{q_e^2 q_m^2} + c_1 q_e^2 + c_1 (q_m^2 + r^2) + \frac{c_2 r}{2(q_e^2 + q_m^2)} + \frac{c_2 (q_e^2 + q_m^2 + r^2) \tan^{-1}\left(\frac{r}{\sqrt{q_e^2 + q_m^2}}\right)}{2(q_e^2 + q_m^2)^{3/2}}. \quad (64)$$

where M denotes the mass of the black hole.

We solve Eqs. (24) and (25) simultaneously to determine the critical electric charge using the metric function (64), which has the value $q_e = 1.725$ if we set the constants $M = 2.0$, $q_m = 0.25$, $c_1 = 1$, and $c_2 = 1$. In the left plot of Fig. 13 we show the behavior of the metric function (64) with respect to the radial coordinate r for three different scenarios of the electric charge: $q_e > q_{ec}$,

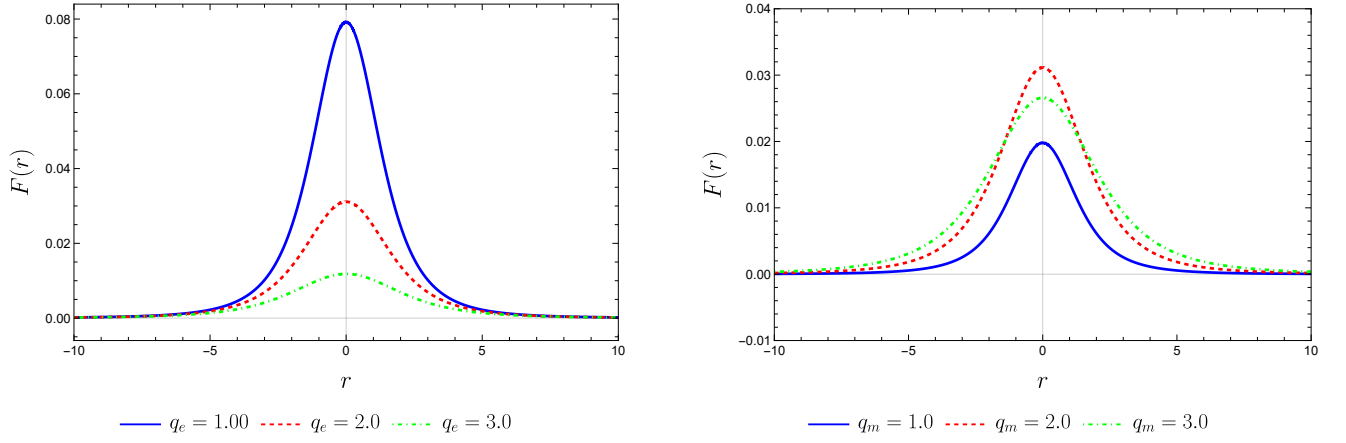


Figure 10. The electromagnetic scalar F , given by Eq. (60), for different values of the electric and magnetic charges. (i) In the left plot, we use the values of the constants as follows $\{q_m = 2.0, c_1 = 1.0, c_2 = 1.0\}$. (ii) In the right plot, we consider $\{q_e = 2.0, c_1 = 1.0, c_2 = 1.0\}$.

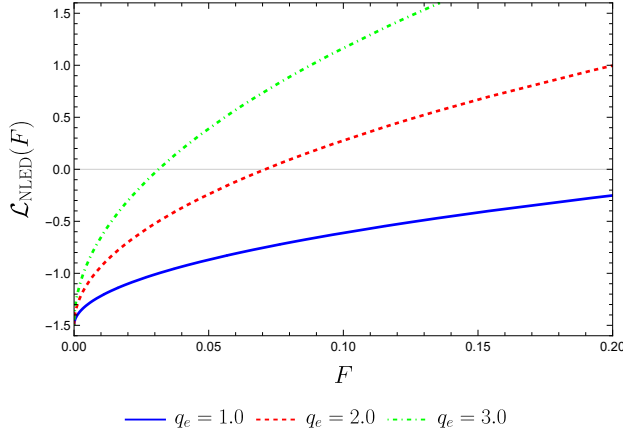


Figure 11. The NLED Lagrangian $\mathcal{L}(F)$, given by Eq. (61) for different values of the electric charge. We have used the values of the constants as follows $\{q_m = 2.0, c_1 = 1.0, c_2 = 1.0\}$.

$q_e = q_{ec}$ and $q_e < q_{ec}$. We note that the behavior in these cases is similar to Fig. 1. Moreover, we emphasize that the asymmetric nature of the metric function becomes clearer if we change the values of the solution parameters.

In the case of the critical magnetic charge, we obtain the value $q_{mc} = 1.888$ by defining the constants $M = 1.0$, $q_e = 0.5$, $c_1 = 1$ and $c_2 = 1$. In the right plot of Fig. 13 we show the behavior of the metric function (64) as a function of the radial coordinate r for three different scenarios of the magnetic charge: $q_m > q_{mc}$, $q_m = q_{mc}$ and $q_m < q_{mc}$. We also note that the behavior in these cases is similar to Fig. 1. In particular, the asymmetric nature of the metric function becomes clearer when we alter the values of the solution's parameters.

Finally, the critical mass, which is determined by simultaneously solving Eqs (24) and (25), takes the value $M_c = 0.138$ if we choose the constant values $q_e = 0.5$,

$q_m = 0.75$, $c_1 = 1$ and $c_2 = 0.12$. Figure 14 shows the behavior of the metric function (64) as a function of the radial coordinate r for three mass scenarios: $M > M_c$, $M = M_c$, and $M < M_c$. We note that the behavior in these cases is similar to that in the right plot of Fig. 1.

Once again, we note that the metric function (64) is not asymptotically flat. However, by defining

$$c_2 = -\frac{4c_1 (q_e^2 + q_m^2)^{3/2}}{\pi}, \quad (65)$$

the Eq. (64) becomes asymptotically flat. Substituting this constant c_2 into (64), we obtain

$$A(r) = 1 - \frac{2M}{\sqrt{q_e^2 + q_m^2 + r^2}} - 4\sqrt{q_e^2 + q_m^2} + c_1 \left(-\frac{2r}{\pi} \sqrt{q_e^2 + q_m^2 + r^2} + q_e^2 + q_m^2 + r^2 \right) - \frac{2c_1}{\pi} (q_e^2 + q_m^2 + r^2) \tan^{-1} \left(\frac{r}{\sqrt{q_e^2 + q_m^2}} \right) \quad (66)$$

Computing the Komar mass via Eq. (27), for the metric function (66), gives

$$M_K = M + \frac{2\bar{c}_1}{3\pi}, \quad (67)$$

where we again substitute $c_1 = -\frac{\bar{c}_1}{(q_e^2 + q_m^2)^{3/2}}$, and \bar{c}_1 is a new positive real constant that is independent of the electric and magnetic charges, so that the Komar mass is also independent of these quantities.

In Fig. 15, we illustrate the behavior of the metric function (66) with two curves. We fix the constants $q_e = 0.1$, $q_m = 0.1$ and $c_2 = 1.0$ for both curves, and vary $c_1 = \pm 1$ to plot the curves with positive and negative c_1 , respectively.

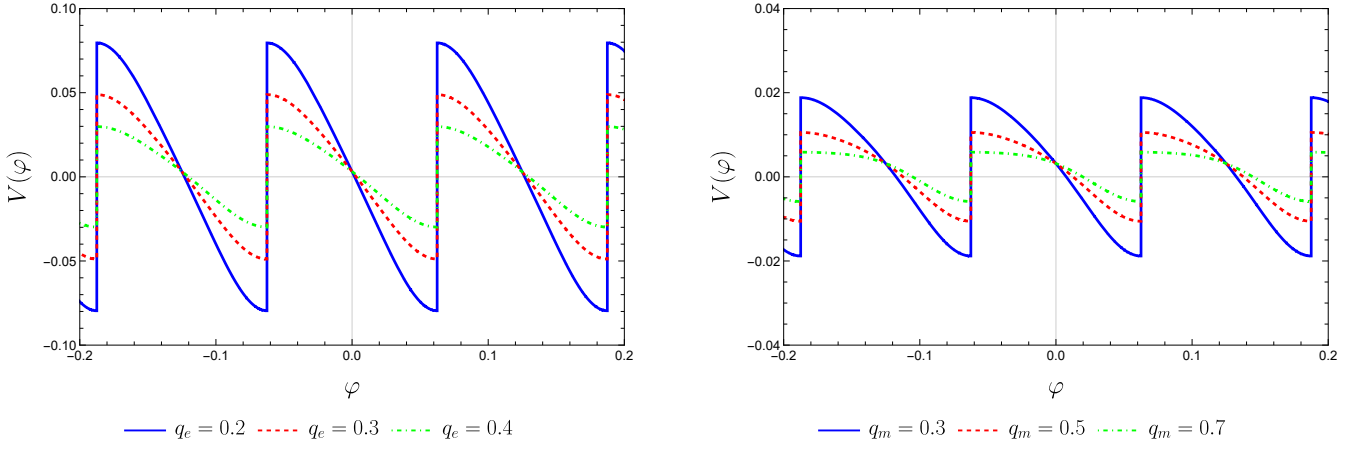


Figure 12. The scalar field potential $V(\varphi)$, described by Eq. (62) for different values of the electric and magnetic charges, taking $\epsilon = -1$. (i) In the left plot, we consider values $\{q_m = 0.3, c_1 = 1.0, c_2 = 1.0\}$. In the right plot, we use the values $\{q_e = 0.5, c_1 = 1.0, c_2 = 1.0\}$.

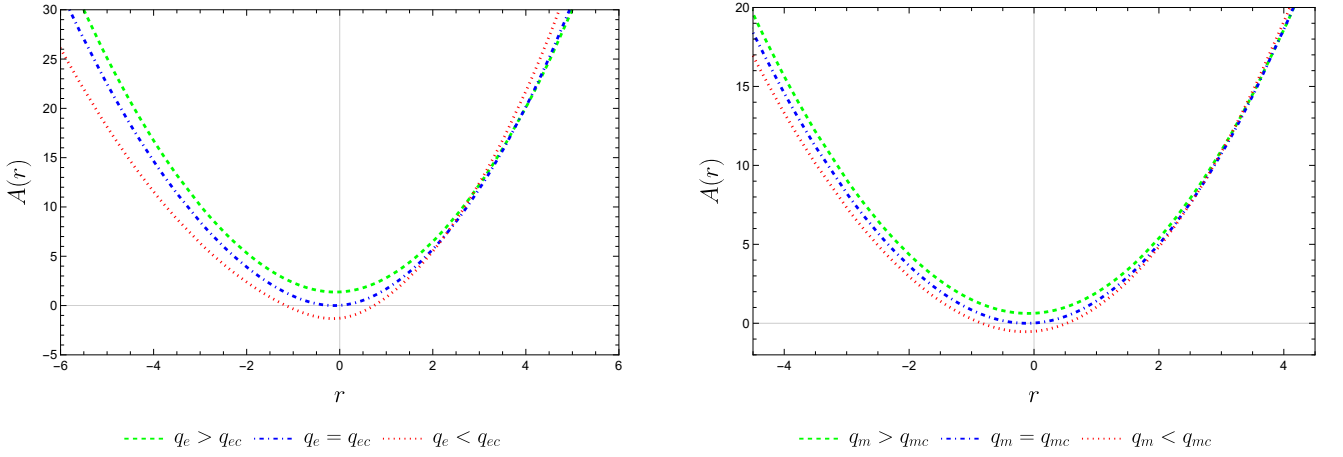


Figure 13. The metric function $A(r)$, given by Eq. (64) for three electric charge scenarios. We have used the values of the constants as follows $\{M = 2.0, q_m = 0.25, c_1 = 1.0, c_2 = 1.0\}$.

B. Kretschmann scalar

We have also calculated the Kretschmann scalar for this solution in order to better examine the regularity of our model. If we take the limit $r \rightarrow 0$ for the Kretschmann scalar, we find that it is regular in the $r \rightarrow 0$ limit

$$\begin{aligned} \lim_{r \rightarrow 0} K(r) = & \left\{ \left[2c_1 (q_e^2 + q_m^2)^3 + 2M (q_e^2 + q_m^2)^{3/2} \right]^2 \right. \\ & + 4 (q_e^2 + q_m^2)^4 + 2 \left[4M (q_e^2 + q_m^2)^{3/2} - 2 (q_e^2 + q_m^2)^2 \right. \\ & + \left. \left. \left(8\sqrt{q_e^2 q_m^2} (q_e^2 + q_m^2)^{3/2} - 2c_1 (q_e^2 + q_m^2)^{5/2} \right) \times \right. \right. \\ & \left. \left. \times \sqrt{q_e^2 + q_m^2} \right]^2 \right\} / (q_e^2 + q_m^2)^6, \end{aligned} \quad (68)$$

while the $r \rightarrow \infty$ limit of the Kretschmann scalar for this solution is also regular

$$\lim_{r \rightarrow \infty} K(r) = \frac{3 \left[4c_1 (q_e^2 + q_m^2) + \pi c_2 \sqrt{\frac{1}{q_e^2 + q_m^2}} \right]^2}{2 (q_e^2 + q_m^2)^2}. \quad (69)$$

We illustrate the behavior of the Kretschmann scalar of this solution in Fig. 16.

C. Matter Lagrangian and Potential reconstruction

Substituting (36) and the metric function (64) into the solution (23), we determine the form of the potential as a function of the radial coordinate for this model, which

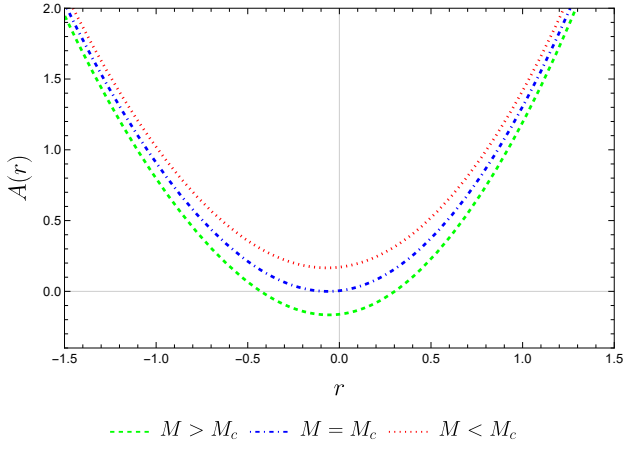


Figure 14. The metric function $A(r)$, given by Eq. (64) for three mass scenarios. We have used the values of the constants as follows $\{q_e = 0.5, q_m = 0.75, c_1 = 1.0, c_2 = 0.12\}$.

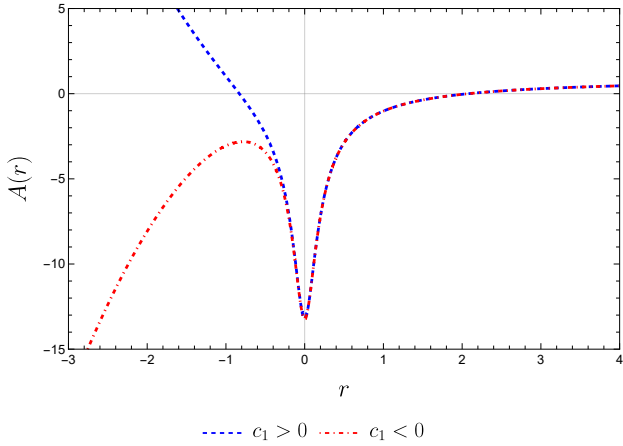


Figure 15. The metric function $A(r)$, given by Eq. (66). We have used the values of the constants as follows $\{q_e = 0.1, q_m = 0.1 \text{ and } M = 1.0\}$.

is given by:

$$V(r) = -\frac{c_2 (q_e^2 + q_m^2 + 3r^2) \tan^{-1}\left(\frac{r}{\sqrt{q_e^2 + q_m^2}}\right)}{2\kappa^2 (q_e^2 + q_m^2)^{3/2} (q_e^2 + q_m^2 + r^2)} + \frac{(4c_1 (q_e^2 + q_m^2)^2 - 3c_2 r)}{2\kappa^2 (q_e^2 + q_m^2) (q_e^2 + q_m^2 + r^2)} + \frac{4m (q_e^2 + q_m^2)}{5\kappa^2 (q_e^2 + q_m^2 + r^2)^{5/2}}. \quad (70)$$

Having used the appropriate quantities such as the function (36), the metric function (64), the scalar field (40) and the potential (70), we can explicitly express the Lagrangian $\mathcal{L}_{\text{NLED}}$ for this model, which is derived from

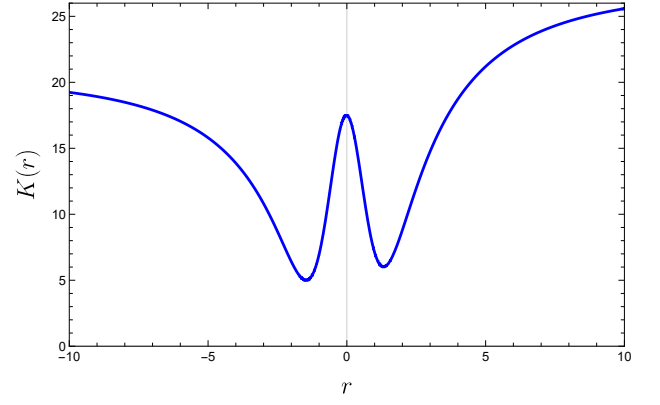


Figure 16. The behavior of the Kretschmann scalar $K(r)$. We have used the values of the constants as follows $\{M = 4.0, q_e = 1.0, q_m = 2.0, c_1 = 1.0, c_2 = 1.0\}$.

the general Lagrangian, given by Eq. (19),

$$\begin{aligned} \mathcal{L}_{\text{NLED}}(r) = & -\frac{3c_1}{2} + \left[\left(\frac{9M^2 (q_e^2 + q_m^2)^2}{q_e^2 + q_m^2 + r^2} \right. \right. \\ & + 24M \sqrt{q_e^2 q_m^2} (q_e^2 + q_m^2) \sqrt{q_e^2 + q_m^2 + r^2} \\ & + 16q_e^2 q_m^2 (q_e^2 + q_m^2 + r^2 - 1) (q_e^2 + q_m^2 + r^2 + 1) \left. \right)^{\frac{1}{2}} \\ & + 4\sqrt{q_e^2 q_m^2} (q_e^2 + q_m^2 + r^2) \left. \right] / 4 (q_e^2 + q_m^2 + r^2)^2 \\ & - \frac{3M (q_e^2 + q_m^2)}{20 (q_e^2 + q_m^2 + r^2)^{5/2}}, \end{aligned} \quad (71)$$

and its derivative \mathcal{L}_F , given by Eq. (20), takes the following form

$$\begin{aligned} \mathcal{L}_F(r) = & \left[\left(24M \sqrt{q_e^2 q_m^2} (q_e^2 + q_m^2) \sqrt{q_e^2 + q_m^2 + r^2} \right. \right. \\ & + 16q_e^2 q_m^2 (q_e^2 + q_m^2 + r^2 - 1) (q_e^2 + q_m^2 + r^2 + 1) \\ & + \frac{9M^2 (q_e^2 + q_m^2)^2}{q_e^2 + q_m^2 + r^2} \left. \right)^{\frac{1}{2}} + \frac{3M (q_e^2 + q_m^2)}{\sqrt{q_e^2 + q_m^2 + r^2}} \\ & + 4\sqrt{q_e^2 q_m^2} (q_e^2 + q_m^2 + r^2) \left. \right] / 4q_m^2. \end{aligned} \quad (72)$$

Taking into account the function (36), the metric function (64), the scalar field (40), the potential (70), the Lagrangian (71), and the derivative of the Lagrangian (72), we can now satisfy all equations (5)–(7) and (15), as well as all components of the equations of motion (16)–(18).

We have also calculated the electromagnetic scalar for this solution and illustrate its behavior in Figs. 17. The left plot depicts three curves corresponding to different values of the electric charge ($q_e = 1.0$, $q_e = 2.0$ and $q_e = 3.0$), similar as depicted in Fig. 4. In the right plot, we

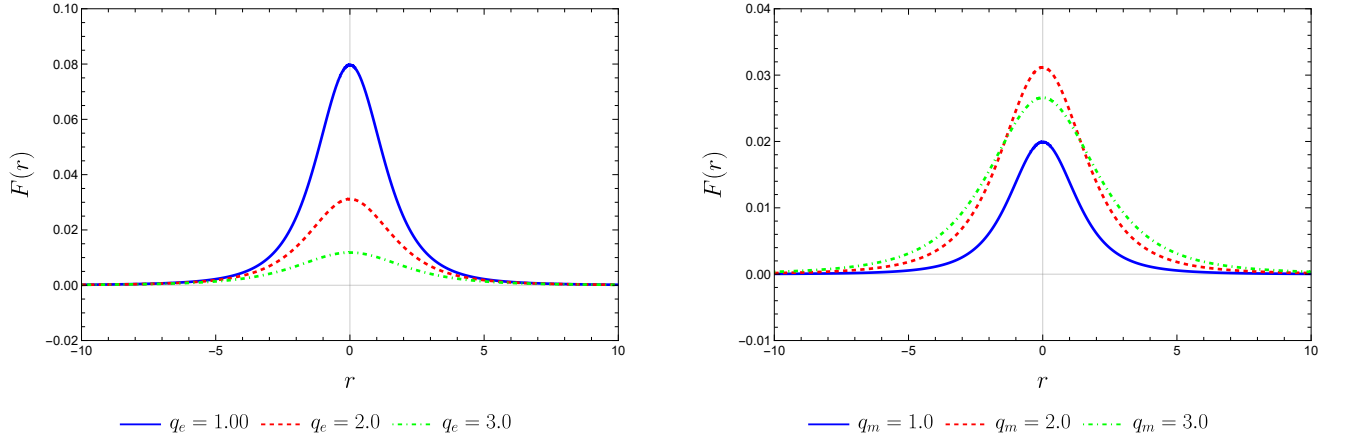


Figure 17. The electromagnetic scalar F , for different values of the electric and magnetic charges. In the left plot, we use the values of the constants as follows $\{M = 4.0, q_m = 2.0, c_1 = 1.0, c_2 = 1.0\}$. In the right plot, we consider the values $\{M = 4.0, q_e = 2.0, c_1 = 1.0, c_2 = 1.0\}$.

analyze the variation of this electromagnetic scalar with the magnetic charge over three different curves ($q_m = 1.0$, $q_m = 2.0$ and $q_m = 3.0$).

By inverting the expression (40), we get $r(\varphi)$ and find

$$\begin{aligned}
 V(\varphi) = & \frac{4M (q_e^2 + q_m^2)}{5\kappa^2 ((q_e^2 + q_m^2) \operatorname{sech}^2(\kappa\varphi\sqrt{\epsilon}))^{5/2}} \\
 & + \frac{\cosh^2(\kappa\varphi\sqrt{\epsilon})}{2\kappa^2} \left(4c_1 - \frac{3c_2 \tan(\varphi\sqrt{\kappa^2(-\epsilon)})}{(q_e^2 + q_m^2)^{3/2}} \right) \\
 & + \frac{c_2 \tan^{-1}\left(\tan(\varphi\sqrt{\kappa^2(-\epsilon)})\right) (\cosh(2\kappa\varphi\sqrt{\epsilon}) - 2)}{2\kappa^2 (q_e^2 + q_m^2)^{3/2}}.
 \end{aligned} \tag{73}$$

In Figs. 18, we illustrate the behavior of the Lagrangian density of NLED as a function of F using parametric graphs for different values of the electric charge ($q_e = 0.3$, $q_e = 0.5$ and $q_e = 0.7$) and the magnetic charge ($q_m = 0.3$, $q_m = 0.5$ and $q_m = 0.7$), respectively. In addition, we present the behavior of the scalar field potential given by Eq. (73) in three different diagrams, each showing three curves with variations of the electric charge ($q_e = 0.2$, $q_e = 0.3$ and $q_e = 0.4$), the magnetic charge ($q_m = 0.3$, $q_m = 0.5$ and $q_m = 0.7$) and the mass ($M = 1.0$, $M = 2.0$ and $M = 3.0$), as shown in Figs. 19. We notice that the amplitude of the potential also varies when we change the values for electric charge, magnetic charge and mass.

VI. FIFTH DYON SOLUTION

A. Metric function and horizons

In this solution, we also require that the Lagrangian described by Eq. (19) is real. To achieve this, we model

the argument root that arises from this Lagrangian according to the following condition:

$$\begin{aligned}
 \Sigma(r)^4 [\Sigma(r)^2 A''(r) - 2A(r) (\Sigma(r)\Sigma''(r) + \Sigma'(r)^2) + 2]^2 \\
 - 64q_e^2 q_m^2 = q_e^2 q_m^2.
 \end{aligned} \tag{74}$$

Again, after considering the function described by Eq. (36), we obtain the following simplified form of the above expression

$$\begin{aligned}
 [A''(r) (q_e^2 + q_m^2 + r^2) - 2A(r) + 2]^2 \times \\
 \times (q_e^2 + q_m^2 + r^2)^2 = 65q_e^2 q_m^2,
 \end{aligned} \tag{75}$$

which yields the following solution for the metric function

$$\begin{aligned}
 A(r) = & \left\{ \left[4c_1 (q_e^2 + q_m^2) (q_e^2 + q_m^2 + r^2) + 2r(c_2 - 2r) \right. \right. \\
 & + \left. \sqrt{65}\sqrt{q_e^2 q_m^2} \right] \times (q_e^2 + q_m^2) + \tan^{-1}\left(\frac{r}{\sqrt{q_e^2 + q_m^2}}\right) \times \\
 & \times 2\sqrt{q_e^2 + q_m^2} \left[c_2 (q_e^2 + q_m^2 + r^2) + \sqrt{65}r\sqrt{q_e^2 q_m^2} \right] + \\
 & \left. \sqrt{65}\sqrt{q_e^2 q_m^2} (q_e^2 + q_m^2 + r^2) \left[\tan^{-1}\left(\frac{r}{\sqrt{q_e^2 + q_m^2}}\right) \right]^2 \right\} \\
 & \times \frac{1}{4(q_e^2 + q_m^2)^2}.
 \end{aligned} \tag{76}$$

We solve Eqs. (24) and (25) simultaneously for this model, determining the critical electric charge from the metric function (76). We obtained the value $q_{ec} = 0.619$, considering the constants defined as: $q_m = 2.0$, $c_1 = -0.13$, and $c_2 = 0.01$. In Fig. 20, we present the behavior of the metric function (76) in relation to the radial coordinate r for three distinct scenarios of the electric charge: $q_e < q_{ec}$, $q_e = q_{ec}$, and $q_e > q_{ec}$. When the charge is less than the critical charge, i.e., $q_e < q_{ec}$, we

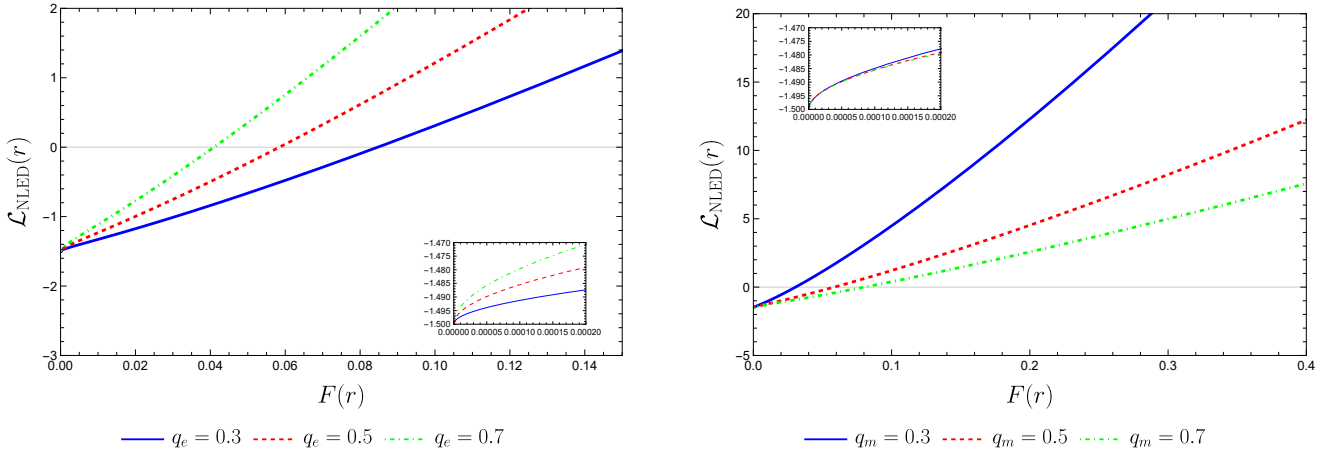


Figure 18. The NLED Lagrangian $\mathcal{L}(F)$, for different values of the electric and magnetic charges. (i) In the left plot, we have used the values of the constants as follows $\{M = 10.0, q_m = 0.5, c_1 = 1.0, c_2 = 1.0\}$. (ii) In the right plot, we consider $\{M = 10.0, q_e = 0.5, c_1 = 1.0, c_2 = 1.0\}$.

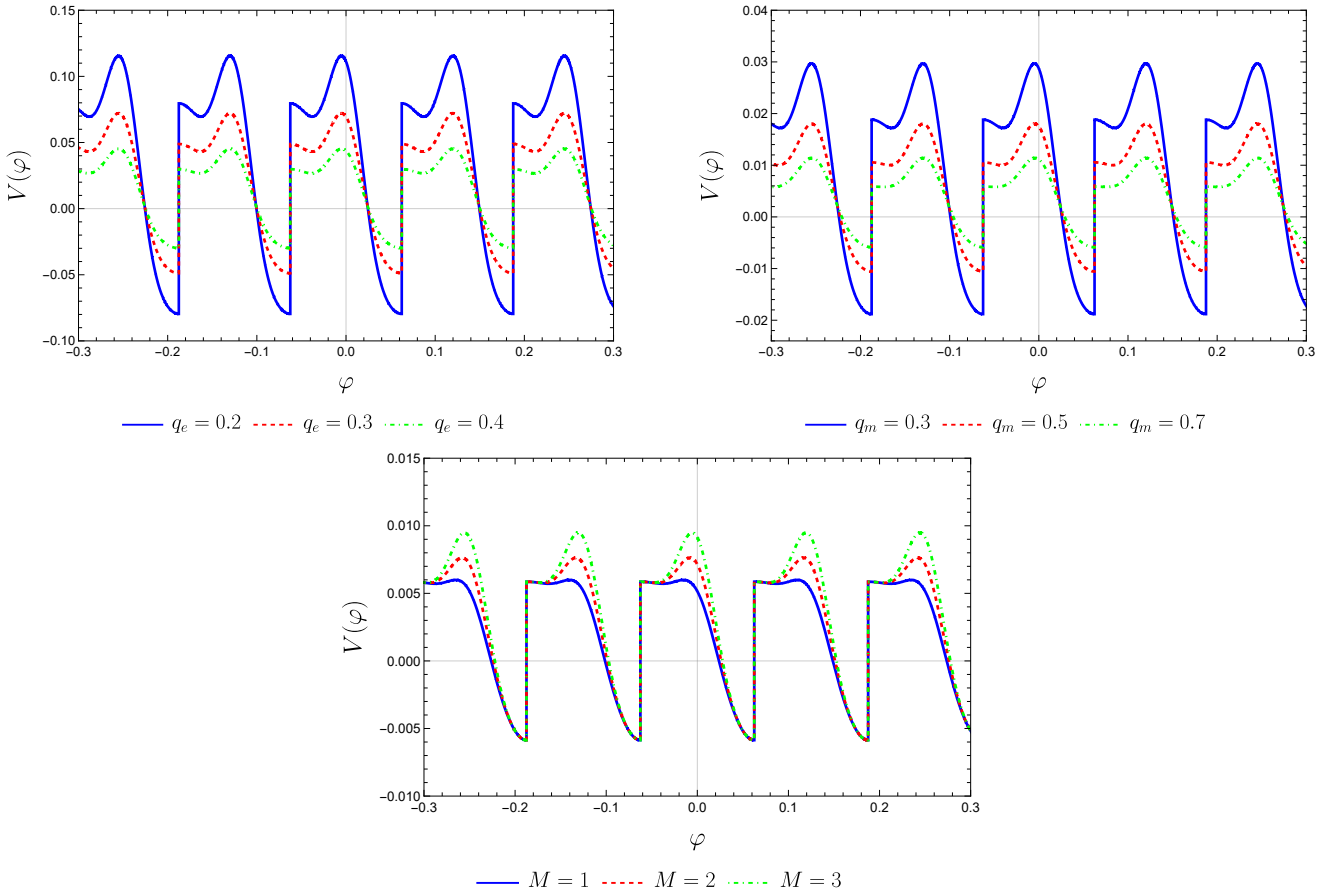


Figure 19. The scalar field potential $V(\varphi)$, described by Eq. (73) taking $\epsilon = -1$. (i) In the left plot, we use the values $\{M = 4.0, q_m = 0.3, c_1 = 1.0, c_2 = 1.0\}$. (ii) In the right plot, we consider $\{M = 4.0, q_e = 0.5, c_1 = 1.0, c_2 = 1.0\}$. (iii) In the bottom plot, we consider $\{q_e = 0.5, q_m = 0.7, c_1 = 1.0, c_2 = 1.0\}$.

observe different behaviors. In the case described by the green curve, the formation of four horizons occurs. In the orange dashed curve, we see the formation of three

horizons. In the black curve, there is only one horizon, while in the purple curve, no horizons are formed. For the critical case, where $q_e = q_{ec}$, we identify the formation

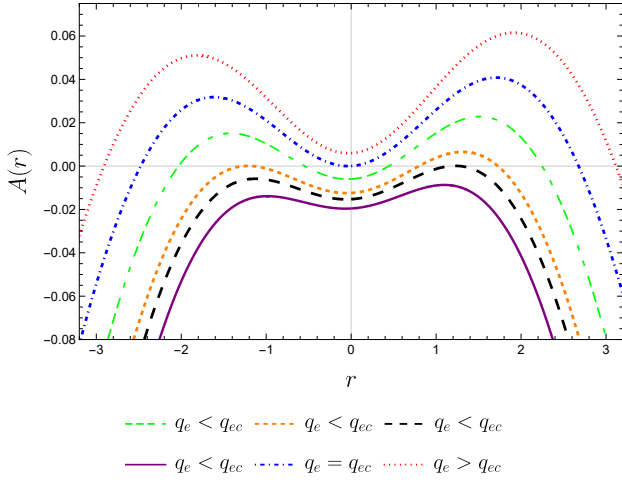


Figure 20. The metric function $A(r)$, given by Eq. (76) for three electric and magnetic charge scenarios. We use the values of the constants as follows $\{q_m = 2.0, c_1 = -0.13, c_2 = 0.01\}$.

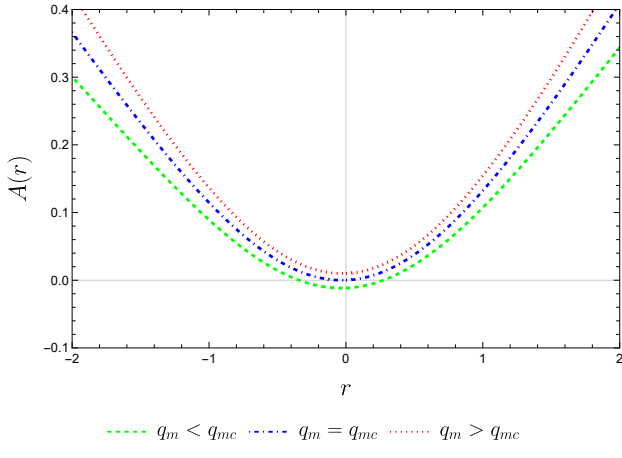


Figure 21. The metric function $A(r)$, given by Eq. (76) for three electric and magnetic charge scenarios. Here, we consider $\{q_e = 1.75, c_1 = -0.205, c_2 = 0.03\}$.

of up to three horizons. Finally, when the electric charge exceeds the critical value, i.e., $q_e > q_{ec}$, the formation of two horizons is observed.

For the critical magnetic charge, we obtained the value $q_m = 0.790$ by defining the constants as $q_e = 1.75$, $c_1 = -0.205$, and $c_2 = 0.03$. In Fig. 21, we present the behavior of the metric function (76) as a function of the radial coordinate r for three different scenarios of the magnetic charge: $q_m > q_{mc}$, $q_m = q_{mc}$, and $q_m < q_{mc}$. In this case, we observe a similar horizon behavior to that of the cases presented in the previous sections.

Once again, we will ensure that the metric function (76) is asymptotically flat. To achieve this, we will now

consider the following expression for the constant c_2

$$c_2 = \left[-16 [c_1 q_e^4 + q_e^2 (2c_1 q_m^2 - 1) + c_1 q_m^4] + 16q_m^2 - \sqrt{65}\pi^2 \sqrt{q_e^2 q_m^2} \right] / \left(4\pi \sqrt{q_e^2 + q_m^2} \right). \quad (77)$$

With this choice, the metric function (76) becomes asymptotically flat. Thus, by substituting the constant (77) into the metric function (76), we obtain the following result

$$A(r) = \frac{1}{8\pi (q_e^2 + q_m^2)^2} \left\{ (q_e^2 + q_m^2)^2 (q_e^2 + q_m^2 + r^2) \times 8\pi c_1 - 16c_1 r (q_e^2 + q_m^2)^{5/2} + \left(2\sqrt{q_e^2 + q_m^2} - \pi r \right) \times \sqrt{q_e^2 + q_m^2} \left(8r \sqrt{q_e^2 + q_m^2} + \pi \sqrt{65} \sqrt{q_e^2 q_m^2} \right) + 2\sqrt{65}\pi \sqrt{q_e^2 q_m^2} (q_e^2 + q_m^2 + r^2) \tan^{-1} \left(\frac{r}{\sqrt{q_e^2 + q_m^2}} \right) + \left[4\sqrt{65}\pi r \sqrt{q_e^2 q_m^2} \sqrt{q_e^2 + q_m^2} + \left[16q_m^2 - 16 (c_1 q_e^4 + q_e^2 (2c_1 q_m^2 - 1) + c_1 q_m^4) - \sqrt{65}\pi^2 \sqrt{q_e^2 q_m^2} \right] \times (q_e^2 + q_m^2 + r^2) \right] \tan^{-1} \left(\frac{r}{\sqrt{q_e^2 + q_m^2}} \right) \right\}. \quad (78)$$

We also calculate the Komar mass, described by Eq. (27), for this metric function, Eq. (78), whose explicit form is now

$$M_K = \frac{\bar{c}_1}{24\pi}, \quad (79)$$

where, we substitute

$$c_1 = \frac{\pi^2 \sqrt{65} \sqrt{q_e^2 q_m^2} + 16q_e^2 + 16q_m^2 - \bar{c}_1 \sqrt{q_e^2 + q_m^2}}{16 (q_e^2 + q_m^2)^2}, \quad (80)$$

and \bar{c}_1 is a new positive real numerical constant independent of the charges q_e and q_m , so that the Komar mass is also independent.

We also calculated the critical magnetic charge based on the metric function described by Eq. (78), obtaining the value $q_m = 0.903$ by setting the constants to $q_e = 0.5$ and $c_1 = -0.75$. In Fig. 22, we illustrate the behavior of the metric function (78) as a function of the radial coordinate r for three different scenarios of the magnetic charge: $q_m > q_{mc}$, $q_m = q_{mc}$, and $q_m < q_{mc}$. We observe that this metric function exhibits asymmetric behavior: for large values of r , the function becomes constant in the region where $r > 0$, whereas in the region where $r < 0$, the function $A(r)$ increases indefinitely.

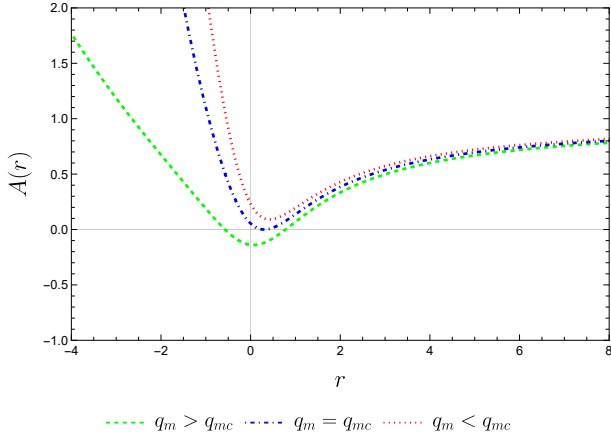


Figure 22. The metric function $A(r)$, given by Eq. (78) for three magnetic charge scenarios. We have used the values of the constants as follows $\{q_e = 0.5, c_1 = -0.75\}$.

B. Kretschmann scalar

We also check the $r \rightarrow 0$ limit for the Kretschmann scalar of this solution, as presented below

$$\lim_{r \rightarrow 0} K(r) = 2c_1 \left(6c_1 + \frac{5\sqrt{65}\sqrt{q_e^2 q_m^2} - 4(q_e^2 + q_m^2)}{(q_e^2 + q_m^2)^2} \right) + \left[715q_m^2 (q_e^2 + q_m^2) + 32(q_e^2 + q_m^2)^2 - 715q_m^4 - 24\sqrt{65}\sqrt{q_e^2 q_m^2} (q_e^2 + q_m^2) \right] / 4(q_e^2 + q_m^2)^4. \quad (81)$$

we observe that, in this limit, the Kretschmann scalar is regular. On the other hand, if we examine the $r \rightarrow \infty$ limit of the Kretschmann scalar, we obtain

$$\lim_{r \rightarrow \infty} K(r) = \frac{3}{32(q_e^2 + q_m^2)^3} \left[\sqrt{\frac{1}{q_e^2 + q_m^2}} \left(16c_1 (q_e^4 + q_m^4) + 16q_e^2 (2c_1 q_m^2 - 1) + \pi^2 \sqrt{65} \sqrt{q_e^2 q_m^2} - 16q_m^2 \right) + 4\pi c_2 \right]^2, \quad (82)$$

and find that the Kretschmann scalar also remains regular in this case.

Although we do not present the explicit form of the Kretschmann scalar for this solution due to its cumbersome algebraic expression, we illustrate its behavior in Fig. 23.

C. Matter Lagrangian and Potential reconstruction

Given the metric function obtained for this solution, Eq. (76) and the function (36), after substituting into

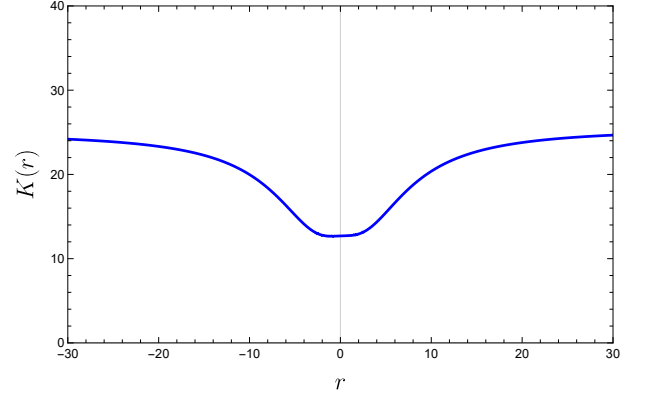


Figure 23. The behavior of the Kretschmann scalar $K(r)$. We have used the values of the constants as follows $\{q_e = 2, q_m = 5, c_1 = c_2 = 1\}$.

the solution (23), we are able to determine the form of the potential in terms of the radial coordinate for this solution, as

$$V(r) = \left\{ 3\sqrt{65}\sqrt{q_e^2 q_m^2} \left[(q_e^2 + q_m^2)^2 - r^4 \right] - 2(q_e^2 + q_m^2) \times \left[8(q_e^2 + q_m^2)^2 [c_1 (q_e^2 + q_m^2) - 1] + \sqrt{65}q_e^2 \sqrt{q_e^2 q_m^2} + \sqrt{65}q_m^2 \sqrt{q_e^2 q_m^2} - 6c_2 r (q_e^2 + q_m^2) - 6c_2 r^3 + 8r^2 \times (q_e^2 + q_m^2) [c_1 (q_e^2 + q_m^2) - 1] \right] + 4(q_e^2 + q_m^2 + r^2) \times \sqrt{q_e^2 + q_m^2} \left[c_2 (q_e^2 + q_m^2 + 3r^2) + 3\sqrt{65}r \sqrt{q_e^2 q_m^2} \right] \times \tan^{-1} \left(\frac{r}{\sqrt{q_e^2 + q_m^2}} \right) + 2\sqrt{65}\sqrt{q_e^2 q_m^2} (q_e^2 + q_m^2 + r^2) \times (q_e^2 + q_m^2 + 3r^2) \tan^{-1} \left(\frac{r}{\sqrt{q_e^2 + q_m^2}} \right)^2 \right\} \times \left(-\frac{1}{8\kappa^2 (q_e^2 + q_m^2)^2 (q_e^2 + q_m^2 + r^2)^2} \right). \quad (83)$$

For this model, we then have the following electromagnetic quantities

$$\mathcal{L}_{\text{NLED}}(r) = -\frac{3}{2}c_1 + \frac{\sqrt{q_e^2 q_m^2}}{8(q_e^2 + q_m^2 + r^2)^2} + \frac{3}{2(q_e^2 + q_m^2)} - \frac{3\sqrt{65}\sqrt{q_e^2 q_m^2}}{16(q_e^2 + q_m^2)^2}, \quad (84)$$

and its derivative \mathcal{L}_F Eq. (20)

$$\mathcal{L}_F(r) = \frac{(\sqrt{65} + 1)\sqrt{q_e^2 q_m^2}}{8q_m^2}. \quad (85)$$

Taking into account the function (36), the metric function (76), the scalar field (40), the potential (83), the Lagrangian (84) and the derivative of the Lagrangian (85),

these satisfy all of equations (5)-(7) and (15), and all components of the equations of motion (16)-(18). Note that the derivative of the Lagrangian we obtain, Eq. (85), depends only on constant quantities.

The electromagnetic scalar for this solution has the form of:

$$F(r) = \frac{q_m^2}{(\sqrt{65} + 1)(q_e^2 + q_m^2 + r^2)^2}. \quad (86)$$

We illustrate the behavior of the electromagnetic scalar (86) in Figs. 24. In the first figure, we plot three curves corresponding to different values of the electric charge ($q_e = 0.2$, $q_e = 0.6$ and $q_e = 1.0$), as depicted in Fig. 24. In the second figure, we analyze the variation of this electromagnetic scalar with the magnetic charge over three different curves ($q_m = 0.2$, $q_m = 0.5$ and $q_m = 0.8$), as shown in the right plot of Fig. 24.

On the other hand, inverting the expressions above to obtain $r(F)$ and $r(\varphi)$, we determine

$$\begin{aligned} \mathcal{L}_{\text{NLED}}(F) = & -\frac{3}{2}c_1 + (\sqrt{65} + 1) \frac{\sqrt{q_e^2 q_m^2} F}{8q_m^2} \\ & + \frac{3 \left(8(q_e^2 + q_m^2) - \sqrt{65} \sqrt{q_e^2 q_m^2} \right)}{16(q_e^2 + q_m^2)^2}. \end{aligned} \quad (87)$$

and

$$\begin{aligned} V(\varphi) = & \left\{ \frac{24c_2 \sqrt{\epsilon} \sqrt{q_e^2 + q_m^2} \sinh(2\kappa\varphi\sqrt{\epsilon})}{\sqrt{-\epsilon}} - 8\sqrt{65} \times \right. \\ & \times \sqrt{q_e^2 q_m^2} [\cosh(2\kappa\varphi\sqrt{\epsilon}) - 2] \tanh^{-1}(\tanh(\kappa\varphi\sqrt{\epsilon}))^2 \\ & + \sqrt{65} \sqrt{q_e^2 q_m^2} [\cosh(4\kappa\varphi\sqrt{\epsilon}) - 8 \cosh(2\kappa\varphi\sqrt{\epsilon})] \\ & + 32(q_e^2 + q_m^2) [c_1(q_e^2 + q_m^2) - 1] [1 + \cosh(2\kappa\varphi\sqrt{\epsilon})] \\ & + \frac{8 \tanh^{-1}[\tanh(\kappa\varphi\sqrt{\epsilon})]}{\kappa\sqrt{\epsilon}} \left[-4c_2 \sqrt{q_e^2 + q_m^2} \sqrt{\kappa^2(-\epsilon)} \right. \\ & + 2c_2 \sqrt{q_e^2 + q_m^2} \sqrt{\kappa^2(-\epsilon)} \cosh(2\kappa\varphi\sqrt{\epsilon}) + 3\sqrt{65} \kappa\sqrt{\epsilon} \times \\ & \left. \left. \times \sqrt{q_e^2 q_m^2} \sinh(2\kappa\varphi\sqrt{\epsilon}) \right] + 3\sqrt{65} \sqrt{q_e^2 q_m^2} \right\} \times \\ & \times \frac{1}{32\kappa^2 (q_e^2 + q_m^2)^2}. \end{aligned} \quad (88)$$

These expressions, Eqs. (87) and (88), represent the material content of this solution. We have obtained a result that was expected to be unequivocal for black-bounce solutions. Specifically, for this class of solutions, when coupling the equations of motion of a given theory with the material content described by NLED and a scalar field, a Lagrangian that is analytically linear, such as the one obtained in this solution and given by Eq. (87), had never been found before. Previously, only analytical nonlinear Lagrangians had been obtained.

In Figs. 25, we illustrate the behavior of the Lagrangian density of NLED as a function of F , Eq. (87),

using plots for different values of the electric charge ($q_e = 1.0$, $q_e = 2.0$ and $q_e = 3.0$) and the magnetic charge ($q_m = 1.0$, $q_m = 2.0$ and $q_m = 3.0$), respectively. We present the behavior of the scalar field potential given by Eq. (88) in three different graphs, each showing three curves with variations of the electric charge ($q_e = 0.2$, $q_e = 0.3$ and $q_e = 0.4$) and the magnetic charge ($q_m = 0.3$, $q_m = 0.5$ and $q_m = 0.7$), as shown in Figs. 26. We notice that the amplitude of the potential also varies when we modify the values for electric charge, magnetic charge and mass.

VII. SUMMARY AND CONCLUSION

In this article, we delved into the study of black-bounce solutions within the context of GR, focusing on static and spherically symmetric geometries. Our primary aim was to explore these solutions by coupling the GR field equations to a combination of NLED and a scalar field, which together act as the source of matter. This approach represents a novel departure from previous studies, which typically consider only magnetic charge or electric charge individually. By incorporating both magnetic and electric charges, we obtain what are known as dyon solutions, offering a more comprehensive view of these intriguing spacetime configurations. We began by presenting the dyon solution within the well-established Reissner-Nordström model, where we do so without including the scalar field as a matter source. In this initial framework, we also calculated the Komar mass associated with this solution, a crucial quantity that we similarly computed for all the subsequent solutions developed. Following this, we expanded on the BB solutions within the dyon context. These solutions introduced a regularization mechanism that avoids the central singularity traditionally present in black hole models, instead featuring a smooth ‘‘bounce’’ at the center. By developing these BB solutions in the presence of both electric and magnetic charges, we offered new insights into the nature of black bounce geometries and their potential to resolve some of the longstanding issues in gravitational physics, particularly regarding singularities and the structure of black holes.

In the first black-bounce model, we explored the solutions by generalizing the Simpson-Visser framework. In this approach, we focused on studying the horizons through numerical solutions, obtained by simultaneously solving the equations (24) and (25). This allowed us to determine the critical parameters: q_{ec} , q_{mc} , and M_c . First, we analyzed the critical charges q_{ec} and q_{mc} . We observed similar behaviors with respect to the horizons:

- No horizon exists for $q_e > q_{ec}$ or $q_m > q_{mc}$.
- When $q_e = q_{ec}$ and $q_m = q_{mc}$, the horizons become degenerate.
- For $q_e < q_{ec}$ and $q_m < q_{mc}$, two horizons appear.

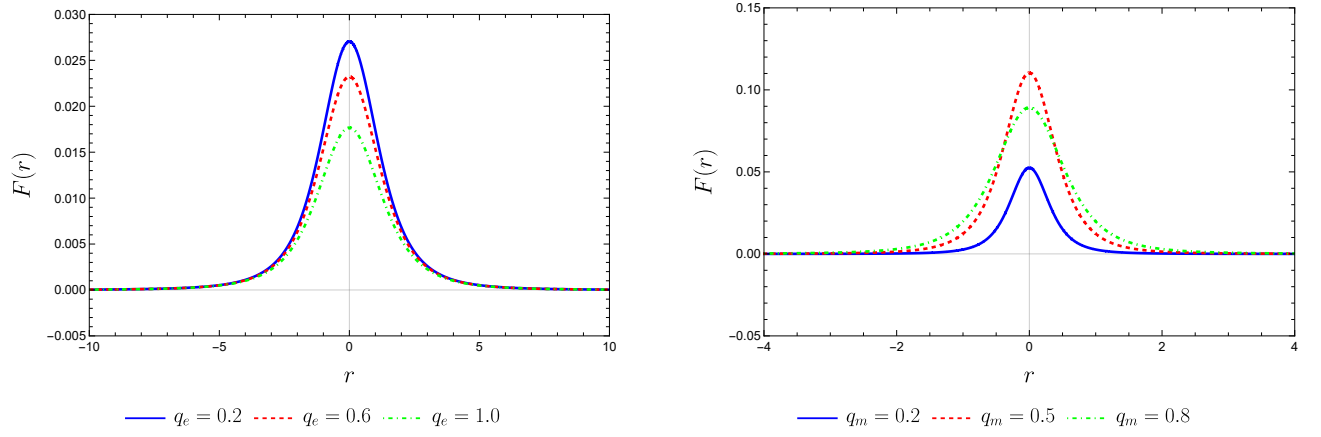


Figure 24. The electromagnetic scalar F , given by Eq. (86), for different values of the electric and magnetic charges. (i) In the left plot, we have used the values of the constants as follows $\{q_m = 2.0, c_1 = 1.0, c_2 = 1.0\}$. In the right plot, we consider the following values $\{q_e = 0.5, c_1 = 1.0, c_2 = 1.0\}$.

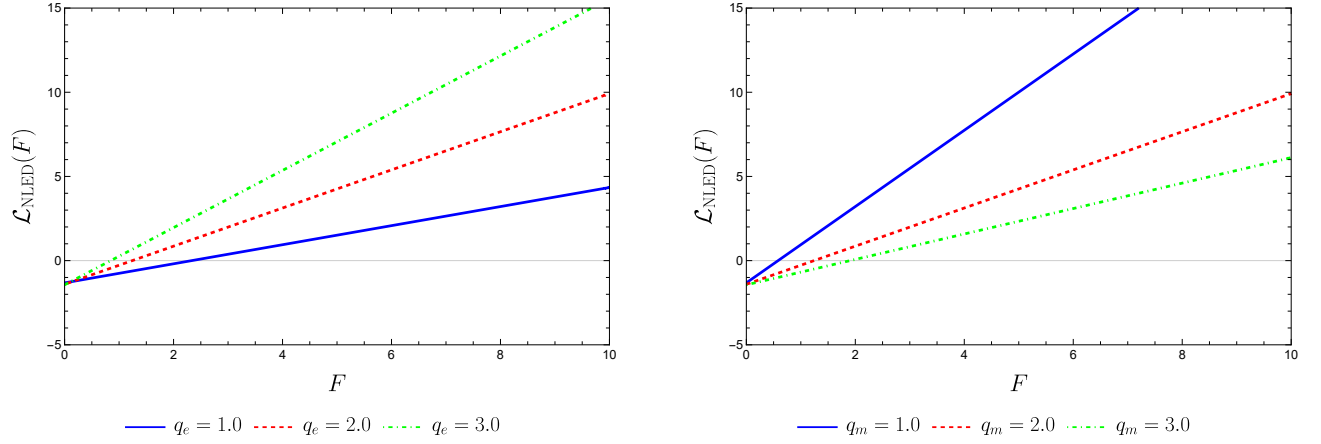


Figure 25. The NLED Lagrangian $\mathcal{L}(F)$, given by Eq. (87) for different values of the electric and magnetic charges. In the left plot, we considered $\{q_e = 1.0, q_e = 2.0, q_e = 3.0\}$, and used the values of the constants as follows $\{q_m = 2.0, c_1 = 1.0\}$. In the right plot, we consider $\{q_m = 1.0, q_m = 2.0, q_m = 3.0\}$, and used the values of the constants as follows $\{q_e = 2.0, c_1 = 1.0\}$.

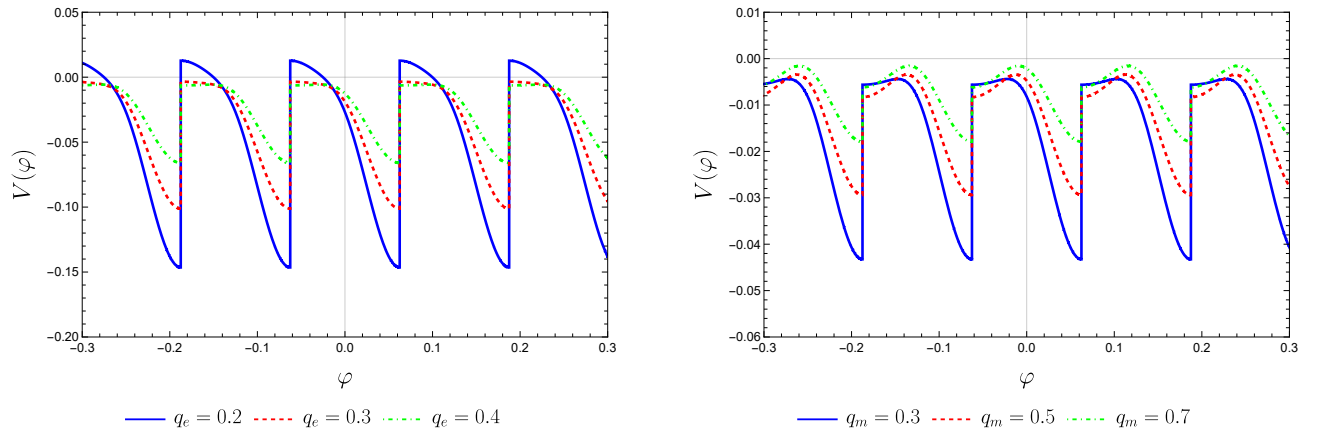


Figure 26. The scalar field potential $V(\varphi)$, described by Eq. (88) for different values of the electric and magnetic charges, taking into account $\epsilon = -1$. (i) In the left plot, we consider $\{q_e = 0.2, q_e = 0.3, q_e = 0.4\}$, for the values $\{q_m = 0.3, c_1 = 1.0, c_2 = 1.0\}$. (ii) In the right plot, we consider $\{q_m = 0.3, q_m = 0.5, q_m = 0.7\}$, for the values $\{q_e = 0.5, c_1 = 1.0, c_2 = 1.0\}$.

Next, we determined the critical mass M_c . For $M > M_c$, a single event horizon is present on both sides of the

bounce at $r = 0$, which merges into a degenerate horizon when $M = M_c$. In contrast, if $M < M_c$, a traversable wormhole forms. We also calculated the Komar mass and found that the metric parameter in this solution coincides with the Komar mass. To further assess the model, we analyzed the Kretschmann scalar, which reveals regularity throughout the entire spacetime. Finally, through direct calculation, we verified that these black-bounce geometries are supported by a specific combination of matter contributions.

In the solutions discussed in Sections IV and VI, we determined the metric function from the Lagrangian expression (19) by imposing the condition that the term under the square root in this expression is a positive real number. Using the resulting metric functions, given by Eqs. (48) and (76), we investigated the possibility of event horizons' existence, depending on the choice of the solution parameters. The behaviors observed were analogous to those found in the Simpson-Visser dyon model. A notable feature that emerged, which was already subtly present in the Simpson-Visser model for our dyon solution, is the evidence of asymmetry in the behavior of the metric functions. This asymmetry is clearly illustrated when comparing the regions $r > 0$ and $r < 0$, particularly through the event horizon curves for the two models. Additionally, we found that, in general, the metric functions of these models, Eqs. (48) and (76), are not asymptotically flat. To achieve asymptotic flatness, we introduced the constants (49) and (77). These constants enabled us to accurately determine the mass or gravitational energy of the system. Consequently, we derived the new metric functions, given by Eqs. (50) and (78), for which we also computed the Komar mass. Finally, as was done in the Simpson-Visser dyon model, we verified the regularity of the Kretschmann scalar in both solutions, confirming its regular behavior throughout the entire spacetime. Furthermore, we determined the explicit forms of the NLED Lagrangian density and the scalar potential that configure these models.

In Section V, we generalized the metric function described by Eq. (48) to incorporate mass into its configuration, as specified in Eq. (64). From this newly obtained metric function, Eq. (64), we investigated the possibility of horizon formation, discovering that the solutions exhibit behavior analogous to that found in the Simpson-Visser dyon model. A key observation is that this metric

function also displays asymmetry in its behavior. As with the previous models, we made the metric function (64) asymptotically flat by choosing the constant c_2 appropriately, as described in Eq. (77). This choice allows us to determine the new metric function, as expressed in Eq. (50), for which we then computed the Komar mass. Finally, we verified the regularity of the Kretschmann scalar for this solution and identified the explicit forms of the NLED Lagrangian density and the scalar potential that structure this model.

To conclude our discussion, we highlight that the model described by the metric function in Eq. (76) offers a novel result in the literature on black bounce solutions. For the first time, a black bounce solution has been derived by coupling a linear Lagrangian from the electromagnetic sector with a scalar field possessing a potential, serving as the matter source. This innovative approach marks a significant step forward in the exploration of non-singular spacetimes. In particular, we observe that the analytical expression for the Lagrangian $\mathcal{L}(F)$ in Eq. (87) is inherently nonlinear, which sets it apart from previous studies that only considered magnetic or electric charges in isolation. Moreover, this previously unexplored aspect of the model presents exciting opportunities for further research. It paves the way for the study of black bounce solutions within the context of dyonic solutions in other modified theories of gravity, offering a promising path toward the development of new, more comprehensive frameworks for understanding gravitational phenomena beyond the singularities traditionally associated with black holes.

ACKNOWLEDGMENTS

MER thanks Conselho Nacional de Desenvolvimento Científico e Tecnológico - CNPq, Brazil, for partial financial support. This study was financed in part by the Coordenação de Aperfeiçoamento de Pessoal de Nível Superior - Brasil (CAPES) - Finance Code 001. FSNL acknowledges support from the Fundação para a Ciência e a Tecnologia (FCT) Scientific Employment Stimulus contract with reference CEECINST/00032/2018, and funding through the research grants UIDB/04434/2020, UIDP/04434/2020 and PTDC/FIS-AST/0054/2021.

-
- [1] A. Einstein, "The foundation of the general theory of relativity.," *Annalen Phys.* **49** (1916) no.7, 769-822.
 - [2] C. M. Will, "New General Relativistic Contribution to Mercury's Perihelion Advance," *Phys. Rev. Lett.* **120** (2018) no.19, 191101 [[arXiv:1802.05304](#) [gr-qc]].
 - [3] C. M. Will, "The 1919 measurement of the deflection of light," *Class. Quant. Grav.* **32** (2015) no.12, 124001 [[arXiv:1409.7812](#) [physics.hist-ph]].
 - [4] B. P. Abbott *et al.* [LIGO Scientific and Virgo], "Observation of Gravitational Waves from a Binary Black Hole Merger," *Phys. Rev. Lett.* **116** (2016) no.6, 061102 [[arXiv:1602.03837](#) [gr-qc]].
 - [5] B. P. Abbott *et al.*, "Multi-messenger Observations of a Binary Neutron Star Merger," *Astrophys. J. Lett.* **848** (2017) no.2, L12 [[arXiv:1710.05833](#) [astro-ph.HE]].
 - [6] K. Akiyama *et al.* [Event Horizon Telescope], "First M87 Event Horizon Telescope Results. I. The Shadow of

- the Supermassive Black Hole,” *Astrophys. J. Lett.* **875** (2019), L1 [[arXiv:1906.11238](#) [astro-ph.GA]].
- [7] K. Akiyama *et al.* [Event Horizon Telescope], “First Sagittarius A* Event Horizon Telescope Results. I. The Shadow of the Supermassive Black Hole in the Center of the Milky Way,” *Astrophys. J. Lett.* **930** (2022) no.2, L12 [[arXiv:2311.08680](#) [astro-ph.HE]].
- [8] S. Antoci and DE Liebscher. Editor’s Note: On the Gravitational Field of a Mass Point According to Einstein’s Theory by K. Schwarzschild. *General Relativity and Gravitation* **35**, 945–950 (2003).
- [9] M. Born and L. Infeld, “Foundations of the new field theory,” *Nature* **132** (1933) no.3348, 1004.1.
- [10] M. Born and L. Infeld, “Foundations of the new field theory,” *Proc. Roy. Soc. Lond. A* **144** (1934) no.852, 425-451.
- [11] W. Heisenberg and H. Euler, “Consequences of Dirac’s theory of positrons,” *Z. Phys.* **98** (1936) no.11-12, 714-732 [[arXiv:physics/0605038](#) [physics]].
- [12] J. Plebanski, *Non-Linear Electrodynamics — A Study* (C.I.E.A. del I.P.N., Mexico City, 1966).
- [13] S. I. Kruglov, “A model of nonlinear electrodynamics,” *Annals Phys.* **353** (2014), 299-306 [[arXiv:1410.0351](#) [physics.gen-ph]].
- [14] S. I. Kruglov, “Nonlinear arcsin-electrodynamics,” *Annalen Phys.* **527** (2015), 397-401 [[arXiv:1410.7633](#) [physics.gen-ph]].
- [15] S. I. Kruglov, “On Generalized Logarithmic Electrodynamics,” *Eur. Phys. J. C* **75** (2015) no.2, 88 [[arXiv:1411.7741](#) [hep-th]].
- [16] I. Bandos, K. Lechner, D. Sorokin and P. K. Townsend, “A non-linear duality-invariant conformal extension of Maxwell’s equations,” *Phys. Rev. D* **102** (2020), 121703 [[arXiv:2007.09092](#) [hep-th]].
- [17] J.M. Bardeen, “Non-singular general-relativistic gravitational collapse,” in *Proceedings of of International Conference GR5,Tbilisi, USSR* (1968), p. 174.
- [18] E. Ayon-Beato and A. Garcia, “The Bardeen model as a nonlinear magnetic monopole,” *Phys. Lett. B* **493** (2000), 149-152 [[arXiv:gr-qc/0009077](#) [gr-qc]].
- [19] M. E. Rodrigues and M. V. de Sousa Silva, “Bardeen Regular Black Hole With an Electric Source,” *JCAP* **06**, 025 (2018) [[arXiv:1802.05095](#) [gr-qc]].
- [20] K. A. Bronnikov, “Regular magnetic black holes and monopoles from nonlinear electrodynamics,” *Phys. Rev. D* **63** (2001), 044005 [[arXiv:gr-qc/0006014](#) [gr-qc]].
- [21] I. Dymnikova, “Regular electrically charged structures in nonlinear electrodynamics coupled to general relativity,” *Class. Quant. Grav.* **21** (2004), 4417-4429 [[arXiv:gr-qc/0407072](#) [gr-qc]].
- [22] L. Balart and E. C. Vagenas, “Regular black holes with a nonlinear electrodynamics source,” *Phys. Rev. D* **90** (2014) no.12, 124045 [[arXiv:1408.0306](#) [gr-qc]].
- [23] H. Culetu, “On a regular charged black hole with a nonlinear electric source,” *Int. J. Theor. Phys.* **54** (2015) no.8, 2855-2863 [[arXiv:1408.3334](#) [gr-qc]].
- [24] N. Breton, “Smarr’s formula for black holes with nonlinear electrodynamics,” *Gen. Rel. Grav.* **37** (2005), 643-650 [[arXiv:gr-qc/0405116](#) [gr-qc]].
- [25] Y. S. Myung, Y. W. Kim and Y. J. Park, “Entropy of an extremal regular black hole,” *Phys. Lett. B* **659** (2008), 832-838 [[arXiv:0705.2478](#) [gr-qc]].
- [26] M. S. Ma, “Magnetically charged regular black hole in a model of nonlinear electrodynamics,” *Annals Phys.* **362** (2015), 529-537 [[arXiv:1509.05580](#) [gr-qc]].
- [27] S. I. Kruglov, “Asymptotic Reissner-Nordström solution within nonlinear electrodynamics,” *Phys. Rev. D* **94** (2016) no.4, 044026 [[arXiv:1608.04275](#) [gr-qc]].
- [28] Z. Y. Fan and X. Wang, “Construction of Regular Black Holes in General Relativity,” *Phys. Rev. D* **94** (2016) no.12, 124027 [[arXiv:1610.02636](#) [gr-qc]].
- [29] L. Balart and E. C. Vagenas, “Regular black hole metrics and the weak energy condition,” *Phys. Lett. B* **730** (2014), 14-17 [[arXiv:1401.2136](#) [gr-qc]].
- [30] S. I. Kruglov, “Nonlinear arcsin-electrodynamics and asymptotic Reissner-Nordström black holes,” *Annalen Phys.* **528** (2016), 588-596 [[arXiv:1607.07726](#) [gr-qc]].
- [31] S. I. Kruglov, “Black hole as a magnetic monopole within exponential nonlinear electrodynamics,” *Annals Phys.* **378** (2017), 59-70 [[arXiv:1703.02029](#) [gr-qc]].
- [32] I. Gullu and S. H. Mazharimousavi, “Double-logarithmic nonlinear electrodynamics,” *Phys. Scripta* **96** (2021) no.4, 045217 [[arXiv:2009.08665](#) [gr-qc]].
- [33] J. S. Schwinger, “Magnetic charge and quantum field theory,” *Phys. Rev.* **144** (1966), 1087-1093.
- [34] M. Kasuya, “Exact Solution of a Rotating Dyon Black Hole,” *Phys. Rev. D* **25** (1982), 995.
- [35] A. Chamorro and K. S. Virbhadra, “A radiating dyon solution,” *Pramana* **45** (1995), 181-187 [[arXiv:hep-th/9406148](#) [hep-th]].
- [36] D. Garfinkle, G. T. Horowitz and A. Strominger, “Charged black holes in string theory,” *Phys. Rev. D* **43** (1991), 3140 [erratum: *Phys. Rev. D* **45** (1992), 3888].
- [37] A. Sen, “Electric magnetic duality in string theory,” *Nucl. Phys. B* **404** (1993), 109-126 [[arXiv:hep-th/9207053](#) [hep-th]].
- [38] G. J. Cheng, R. R. Hsu and W. F. Lin, “Dyonic black holes in string theory,” *J. Math. Phys.* **35** (1994), 4839-4847 [[arXiv:hep-th/9302065](#) [hep-th]].
- [39] S. Mignemi, “Dyonic black holes in effective string theory,” *Phys. Rev. D* **51** (1995), 934-937 [[arXiv:hep-th/9303102](#) [hep-th]].
- [40] D. A. Lowe and A. Strominger, “Exact four-dimensional dyonic black holes and Bertotti-Robinson space-times in string theory,” *Phys. Rev. Lett.* **73** (1994), 1468-1471 [[arXiv:hep-th/9403186](#) [hep-th]].
- [41] D. P. Jatkar, S. Mukherji and S. Panda, “Dyonic black hole in heterotic string theory,” *Nucl. Phys. B* **484** (1997), 223-244 [[arXiv:hep-th/9512157](#) [hep-th]].
- [42] M. Cvetič and A. A. Tseytlin, “Solitonic strings and BPS saturated dyonic black holes,” *Phys. Rev. D* **53** (1996), 5619-5633 [erratum: *Phys. Rev. D* **55** (1997), 3907] [[arXiv:hep-th/9512031](#) [hep-th]].
- [43] A. A. Tseytlin, “Extreme dyonic black holes in string theory,” *Mod. Phys. Lett. A* **11** (1996), 689-714 [[arXiv:hep-th/9601177](#) [hep-th]].
- [44] A. H. Chamseddine and W. A. Sabra, “Magnetic and dyonic black holes in $D = 4$ gauged supergravity,” *Phys. Lett. B* **485** (2000), 301-307 [[arXiv:hep-th/0003213](#) [hep-th]].
- [45] D. D. K. Chow and G. Compère, “Dyonic AdS black holes in maximal gauged supergravity,” *Phys. Rev. D* **89** (2014) no.6, 065003 [[arXiv:1311.1204](#) [hep-th]].
- [46] H. Lü, Y. Pang and C. N. Pope, “AdS Dyonic Black Hole and its Thermodynamics,” *JHEP* **11** (2013), 033 [[arXiv:1307.6243](#) [hep-th]].
- [47] A. Guarino, D. L. Jafferis and O. Varela, “String Theory Origin of Dyonic $N=8$ Supergravity and Its Chern-

- Simons Duals,” *Phys. Rev. Lett.* **115** (2015) no.9, 091601 [[arXiv:1504.08009](#) [hep-th]].
- [48] F. Benini, K. Hristov and A. Zaffaroni, “Exact microstate counting for dyonic black holes in AdS₄,” *Phys. Lett. B* **771** (2017), 462-466 [[arXiv:1608.07294](#) [hep-th]].
- [49] P. Meessen, T. Ortín and P. F. Ramírez, “Dyonic black holes at arbitrary locations,” *JHEP* **10** (2017), 066 [[arXiv:1707.03846](#) [hep-th]].
- [50] A. D. Shapere, S. Trivedi and F. Wilczek, “Dual dilaton dyons,” *Mod. Phys. Lett. A* **6** (1991), 2677-2686.
- [51] S. J. Poletti, J. Twamley and D. L. Wiltshire, “Dyonic Dilaton black holes,” *Class. Quant. Grav.* **12** (1995), 1753-1770 [erratum: *Class. Quant. Grav.* **12** (1995), 2355] [[arXiv:hep-th/9502054](#) [hep-th]].
- [52] Y. Brihaye, B. Hartmann and J. Kunz, “Gravitating dyons and dyonic black holes,” *Phys. Lett. B* **441** (1998), 77-82 [[arXiv:hep-th/9807169](#) [hep-th]].
- [53] G. Lopes Cardoso, B. de Wit, J. Kappeli and T. Mohaupt, “Asymptotic degeneracy of dyonic $N = 4$ string states and black hole entropy,” *JHEP* **12** (2004), 075 [[arXiv:hep-th/0412287](#) [hep-th]].
- [54] S. A. Hartnoll and P. Kovtun, “Hall conductivity from dyonic black holes,” *Phys. Rev. D* **76** (2007), 066001 [[arXiv:0704.1160](#) [hep-th]].
- [55] S. A. Hartnoll, P. K. Kovtun, M. Muller and S. Sachdev, “Theory of the Nernst effect near quantum phase transitions in condensed matter, and in dyonic black holes,” *Phys. Rev. B* **76** (2007), 144502 [[arXiv:0706.3215](#) [cond-mat.str-el]].
- [56] T. Albash and C. V. Johnson, “A Holographic Superconductor in an External Magnetic Field,” *JHEP* **09** (2008), 121 [[arXiv:0804.3466](#) [hep-th]].
- [57] C. M. Chen, D. V. Gal’tsov and D. G. Orlov, “Extremal dyonic black holes in D=4 Gauss-Bonnet gravity,” *Phys. Rev. D* **78** (2008), 104013 [[arXiv:0809.1720](#) [hep-th]].
- [58] M. M. Caldarelli, O. J. C. Dias and D. Klemm, “Dyonic AdS black holes from magnetohydrodynamics,” *JHEP* **03** (2009), 025 [[arXiv:0812.0801](#) [hep-th]].
- [59] C. M. Chen, Y. M. Huang, J. R. Sun, M. F. Wu and S. J. Zou, “On Holographic Dual of the Dyonic Reissner-Nordstrom Black Hole,” *Phys. Rev. D* **82** (2010), 066003 [[arXiv:1006.4092](#) [hep-th]].
- [60] S. Dutta, A. Jain and R. Soni, “Dyonic Black Hole and Holography,” *JHEP* **12** (2013), 060 [[arXiv:1310.1748](#) [hep-th]].
- [61] R. G. Cai and R. Q. Yang, “Paramagnetism-Ferromagnetism Phase Transition in a Dyonic Black Hole,” *Phys. Rev. D* **90** (2014) no.8, 081901 [[arXiv:1404.2856](#) [hep-th]].
- [62] S. Li, H. Lu and H. Wei, “Dyonic (A)dS Black Holes in Einstein-Born-Infeld Theory in Diverse Dimensions,” *JHEP* **07** (2016), 004 [[arXiv:1606.02733](#) [hep-th]].
- [63] S. H. Hendi, N. Riazi and S. Panahiyan, “Holographical aspects of dyonic black holes: Massive gravity generalization,” *Annalen Phys.* **530** (2018) no.2, 1700211 [[arXiv:1610.01505](#) [hep-th]].
- [64] K. A. Bronnikov, “Dyonic configurations in nonlinear electrodynamics coupled to general relativity,” *Grav. Cosmol.* **23** (2017) no.4, 343-348 [[arXiv:1708.08125](#) [gr-qc]].
- [65] C. Bambi, “Regular Black Holes. Towards a New Paradigm of Gravitational Collapse,” Springer, 2023, ISBN 978-981-99-1595-8, 978-981-99-1598-9, 978-981-99-1596-5 [[arXiv:2307.13249](#) [gr-qc]].
- [66] A. Simpson and M. Visser, “Black-bounce to traversable wormhole,” *JCAP* **02** (2019), 042 [[arXiv:1812.07114](#) [gr-qc]].
- [67] F. S. N. Lobo, M. E. Rodrigues, M. V. de Sousa Silva, A. Simpson and M. Visser, “Novel black-bounce spacetimes: wormholes, regularity, energy conditions, and causal structure,” *Phys. Rev. D* **103** (2021) no.8, 084052 [[arXiv:2009.12057](#) [gr-qc]].
- [68] J. R. Nascimento, A. Y. Petrov, P. J. Porfirio and A. R. Soares, “Gravitational lensing in black-bounce spacetimes,” *Phys. Rev. D* **102** (2020) no.4, 044021 [[arXiv:2005.13096](#) [gr-qc]].
- [69] N. Tsukamoto, “Gravitational lensing in the Simpson-Visser black-bounce spacetime in a strong deflection limit,” *Phys. Rev. D* **103** (2021) no.2, 024033 [[arXiv:2011.03932](#) [gr-qc]].
- [70] X. T. Cheng and Y. Xie, “Probing a black-bounce, traversable wormhole with weak deflection gravitational lensing,” *Phys. Rev. D* **103**, no.6, 064040 (2021).
- [71] “Gravitational lensing by two photon spheres in a black-bounce spacetime in strong deflection limits,” *Phys. Rev. D* **104** (2021) no.6, 064022 [[arXiv:2105.14336](#) [gr-qc]].
- [72] J. Zhang and Y. Xie, “Gravitational lensing by a black-bounce-Reissner-Nordström spacetime,” *Eur. Phys. J. C* **82** (2022) no.5, 471.
- [73] M. Guerrero, G. J. Olmo, D. Rubiera-Garcia and D. S. C. Gómez, “Shadows and optical appearance of black bounces illuminated by a thin accretion disk,” *JCAP* **08** (2021), 036 [[arXiv:2105.15073](#) [gr-qc]].
- [74] K. Jafarzade, M. Kord Zangeneh and F. S. N. Lobo, “Observational optical constraints of regular black holes,” *Annals Phys.* **446** (2022), 169126 [[arXiv:2106.13893](#) [gr-qc]].
- [75] K. Jafarzade, M. Kord Zangeneh and F. S. N. Lobo, “Shadow, deflection angle and quasinormal modes of Born-Infeld charged black holes,” *JCAP* **04** (2021), 008 [[arXiv:2010.05755](#) [gr-qc]].
- [76] K. Jafarzade, M. Kord Zangeneh and F. S. N. Lobo, “Optical Features of AdS Black Holes in the Novel 4D Einstein-Gauss-Bonnet Gravity Coupled to Non-linear Electrodynamics,” *Universe* **8** (2022) no.3, 182 [[arXiv:2009.12988](#) [gr-qc]].
- [77] Y. Yang, D. Liu, Z. Xu, Y. Xing, S. Wu and Z. W. Long, “Echoes of novel black-bounce spacetimes,” *Phys. Rev. D* **104** (2021) no.10, 104021 [[arXiv:2107.06554](#) [gr-qc]].
- [78] P. Bambhaniya, S. K. K. Jusufi and P. S. Joshi, “Thin accretion disk in the Simpson-Visser black-bounce and wormhole spacetimes,” *Phys. Rev. D* **105** (2022) no.2, 023021 [[arXiv:2109.15054](#) [gr-qc]].
- [79] M. Y. Ou, M. Y. Lai and H. Huang, “Echoes from asymmetric wormholes and black bounce,” *Eur. Phys. J. C* **82** (2022) no.5, 452 [[arXiv:2111.13890](#) [gr-qc]].
- [80] Y. Guo and Y. G. Miao, “Charged black-bounce spacetimes: Photon rings, shadows and observational appearances,” *Nucl. Phys. B* **983** (2022), 115938 [[arXiv:2112.01747](#) [gr-qc]].
- [81] S. R. Wu, B. Q. Wang, D. Liu and Z. W. Long, “Echoes of charged black-bounce spacetimes,” *Eur. Phys. J. C* **82** (2022) no.11, 998 [[arXiv:2201.08415](#) [gr-qc]].
- [82] N. Tsukamoto, “Retrolensing by two photon spheres of a black-bounce spacetime,” *Phys. Rev. D* **105** (2022) no.8, 084036 [[arXiv:2202.09641](#) [gr-qc]].
- [83] J. Mazza, E. Franzin and S. Liberati, “A novel family of rotating black hole mimickers,” *JCAP* **04** (2021), 082

- [arXiv:2102.01105 [gr-qc]].
- [84] Z. Xu and M. Tang, “Rotating spacetime: black-bounces and quantum deformed black hole,” *Eur. Phys. J. C* **81** (2021) no.10, 863 [arXiv:2109.13813 [gr-qc]].
- [85] K. A. Bronnikov, “Black bounces, wormholes, and partly phantom scalar fields,” *Phys. Rev. D* **106** (2022) no.6, 064029 [arXiv:2206.09227 [gr-qc]].
- [86] P. Cañate, “Black bounces as magnetically charged phantom regular black holes in Einstein-nonlinear electrodynamics gravity coupled to a self-interacting scalar field,” *Phys. Rev. D* **106** (2022) no.2, 024031 [arXiv:2202.02303 [gr-qc]].
- [87] M. E. Rodrigues and M. V. d. S. Silva, “Source of black bounces in general relativity,” *Phys. Rev. D* **107** (2023) no.4, 044064 [arXiv:2302.10772 [gr-qc]].
- [88] C. F. S. Pereira, D. C. Rodrigues, J. C. Fabris and M. E. Rodrigues, “Black-bounce solution in k-essence theories,” *Phys. Rev. D* **109** (2024) no.4, 044011 [arXiv:2309.10963 [gr-qc]].
- [89] G. Alencar, K. A. Bronnikov, M. E. Rodrigues, D. Sáez-Chillón Gómez and M. V. de S. Silva, “On black bounce space-times in non-linear electrodynamics,” *Eur. Phys. J. C* **84** (2024) no.7, 745 [arXiv:2403.12897 [gr-qc]].
- [90] A. Komar, “Covariant conservation laws in general relativity,” *Phys. Rev.* **113** (1959), 934-936.